

# Collisional Cascades in Planetesimal Disks I. Stellar Flybys

Scott J. Kenyon

*Smithsonian Astrophysical Observatory, 60 Garden Street, Cambridge, MA 02138*

e-mail: skenyon@cfa.harvard.edu

Benjamin C. Bromley

*Department of Physics, University of Utah, 201 JFB, Salt Lake City, UT 84112*

e-mail: bromley@physics.utah.edu

## ABSTRACT

We use a new multiannulus planetesimal accretion code to investigate the evolution of a planetesimal disk following a moderately close encounter with a passing star. The calculations include fragmentation, gas and Poynting-Robertson drag, and velocity evolution from dynamical friction and viscous stirring. We assume that the stellar encounter increases planetesimal velocities to the shattering velocity, initiating a collisional cascade in the disk. During the early stages of our calculations, erosive collisions damp particle velocities and produce substantial amounts of dust. For a wide range of initial conditions and input parameters, the time evolution of the dust luminosity follows a simple relation,  $L_d/L_\star = L_0/[\alpha + (t/t_d)^\beta]$ . The maximum dust luminosity  $L_0$  and the damping time  $t_d$  depend on the disk mass, with  $L_0 \propto M_d$  and  $t_d \propto M_d^{-1}$ . For disks with dust masses of 1% to 100% of the ‘minimum mass solar nebula’ (1–100  $M_\oplus$  at 30–150 AU), our calculations yield  $t_d \sim 1$ –10 Myr,  $\alpha \approx 1$ –2,  $\beta = 1$ , and dust luminosities similar to the range observed in known ‘debris disk’ systems,  $L_0 \sim 10^{-3}$  to  $10^{-5}$ . Less massive disks produce smaller dust luminosities and damp on longer timescales. Because encounters with field stars are rare, these results imply that moderately close stellar flybys cannot explain collisional cascades in debris disk systems with stellar ages of  $\sim 100$  Myr or longer.

*Subject headings:* planetary systems – solar system: formation – stars: formation – circumstellar matter

## 1. INTRODUCTION

Many nearby main sequence stars have thermal emission from cold dust (Backman & Paresce 1993; Artymowicz 1997; Lagrange et al. 2000). These ‘debris disk’ systems often have a disk-like

or ring morphology at optical or infrared wavelengths, with typical radii of 50–1000 AU (e.g., Smith & Terrile 1984; Greaves et al. 1998; Holland et al. 1998; Jayawardhana et al. 1998; Koerner et al. 1998; Schneider et al. 1999; Weinberger et al. 1999). The near-IR and far-IR excess emission is a small fraction of the stellar luminosity; the ratio of the total dust luminosity to the stellar luminosity is  $L_d/L_\star \sim 10^{-5}$  to  $10^{-2}$  in most systems (Aumann et al. 1984; Fajardo-Acosta et al. 1999; Habing et al. 1999; Spangler et al. 2001). Recent studies indicate that the dust luminosity declines on timescales of 10–100 Myr (Barrado y Navascués et al. 1999; Habing et al. 1999; Song et al. 2000b). Kalas (1998) and Spangler et al. (2001) propose power-law relations for this decline,  $L_d \propto t^{-1}$  (Kalas 1998) and  $L_d \propto t^{-2}$  (Spangler et al. 2001).

In current theories, dynamic processes produce dust emission in a debris disk. If the disk contains small dust grains with sizes of 1–100  $\mu\text{m}$  and a total mass in small grains of  $\sim 0.01 M_\oplus^1$ , radiative transfer models can explain both the scattered-light images and the spectral energy distributions of most systems (e.g., Backman & Paresce 1993; Artymowicz 1997, Greaves, Mannings, & Holland 2000b). However, radiation pressure and Poynting-Robertson drag remove small grains from the disk on short timescales,  $\sim 1$ –10 Myr, compared to the age of a typical system. Collisions between larger bodies can replenish the small grain population when their relative velocities are large enough to begin a ‘collisional cascade,’ where 1–10 km planetesimals are ground down into smaller and smaller bodies. If planetesimal velocities are close to the ‘shattering velocity’ of  $\sim 200 \text{ m s}^{-1}$  and if the mass in 1–10 km planetesimals is  $\sim 100 M_\oplus$ , collisional cascades can maintain the observed small grain population over timescales of  $\sim 100$  Myr or longer (Habing et al. 1999; Greaves, et al. 2000b; Kenyon & Bromley 2001).

At least two mechanisms can produce large collision velocities in a debris disk. During the early evolution of the disk, there is a strong coupling between solid bodies and the gas; circularization is efficient and collision velocities are low. As solid bodies in the disk merge and grow, impulsive encounters with passing stars or stirring by large planets embedded in the disk can increase collision velocities (Artymowicz et al. 1989; Mouillet et al. 1997; Ida et al. 2000; Kalas et al. 2000). Kenyon & Bromley (2001) show that embedded planets with radii of 500 km or larger can dynamically heat smaller bodies to the shattering velocity on timescales of 10–100 Myr. Collisions between 1–10 km objects can then replenish the small grain population for  $\sim 500$  Myr or longer (see also Kenyon 2002). Ida et al. (2000) and Kalas et al. (2000) use  $n$ -body simulations to demonstrate that close encounters between the disk and a passing star can excite large particle velocities in the disk. Because the growth of large planets in the outer disk is unlikely, these ‘stellar flybys’ are an attractive way to induce collisional cascades in the large disks observed in  $\beta$  Pic and other nearby stars. The evolution of a particle disk after the stellar flyby is uncertain. Collisions of small bodies in the disk may damp planetesimal velocities and thus halt the collisional cascade. Kenyon & Luu (1999) derive damping times of 1–10 Myr for 1–100 m planetesimals in the Kuiper Belt. If this timescale is typical, then stellar flybys can explain debris disks only if the encounters

---

<sup>1</sup>1  $M_\oplus = 6 \times 10^{27}$  g is the mass of the earth

are frequent.

Here we investigate the evolution of a planetesimal disk following a moderately close stellar flyby. We use a new multi-annulus planetesimal evolution code to compute the collisional and dynamical evolution of small bodies in an extended disk surrounding an intermediate mass star. Calculations for disks with dust masses comparable to the ‘minimum mass solar nebula’ ( $\sim 100 M_{\oplus}$  of solid material at 30–150 AU) show that two body collisions can damp planetesimal velocities on timescales of 1–10 Myr. Less massive disks damp on longer timescales. Small dust grains generated in the collisional cascade produce a significant luminosity, with  $L_d/L_{\star} \sim 5 \times 10^{-2}$  for a minimum mass solar nebula. Less massive disks yield smaller dust luminosities. These results suggest that stellar flybys cannot initiate luminous, long-lived collisional cascades in a planetesimal disk. Unless all known debris disk systems have had a stellar encounter in the past 10–100 Myr, a nearby binary companion star or planets embedded in the disk probably initiated the collisional cascades in these systems.

We outline the model in §2, describe the calculations in §3, and conclude with a brief discussion in §4.

## 2. THE MODEL

We treat planetesimals as a statistical ensemble of masses with a distribution of horizontal and vertical velocities about a Keplerian orbit (Safronov 1969; Wetherill & Stewart 1989; Kenyon & Luu 1998, 1999, and references therein). The model grid contains  $N$  concentric annuli centered at heliocentric distances  $a_i$ . Each annulus has an inner radius at  $a_i - \delta a_i/2$  and an outer radius at  $a_i + \delta a_i/2$ . The midpoint of the model grid is at a heliocentric distance  $a_{mid}$ . Calculations begin with a differential mass distribution  $n(m_{ik})$  of bodies with horizontal and vertical velocities  $h_{ik}(t)$  and  $v_{ik}(t)$ .

To evolve the mass and velocity distributions in time, we solve the coagulation and the Fokker-Planck equations for an ensemble of masses undergoing inelastic collisions, drag forces, and dynamical friction and viscous stirring. We approximate collision cross-sections using the particle-in-a-box formalism and treat gas and Poynting-Robertson drag with simple analytic formulae (see the Appendix). Kenyon & Bromley (2001) outline our treatment of elastic gravitational interactions (see also Spaute et al. 1991; Weidenschilling et al. 1997).

We allow four collision outcomes (Greenberg et al. 1978; Davis et al. 1985; Barge & Pellat 1993; Wetherill & Stewart 1993):

1. Mergers – two bodies collide and merge into a single object with no debris;
2. Cratering – two bodies merge into a single object but produce debris with mass of 20% or less of the mass of the merged object;

3. Rebounds – two bodies collide and produce some debris but do not merge into a single object; and
4. Disruption – two bodies collide and produce debris with a mass comparable to the mass of the two initial bodies.

The appendix of Kenyon & Luu (1999) describes the algorithm for specifying the outcome as a function of the collision velocity, the tensile strength of the colliding bodies  $S_0$ , and other physical parameters. For the calculations described in this paper, all collisions result in debris; rebounds are unimportant. For most calculations, we adopt  $S_0 = 2 \times 10^6$  erg g<sup>-1</sup> and a crushing energy  $Q_c = 5 \times 10^7$  erg g<sup>-1</sup>, appropriate for icy objects at large distances from the central star (see Kenyon & Luu 1999, and references therein).

The initial conditions for these calculations are appropriate for a disk with an age of  $\sim 10$  Myr. We consider systems of  $N$  annuli in disks with  $a_{mid} = 35\text{--}140$  AU and  $\delta a_i/a_i = 0.01\text{--}0.025$ . The disk is composed of small planetesimals with radii of  $\sim 1\text{--}100$  m (see below). The particles have an initial mass distribution  $n_i(m_k)$  in each annulus and begin with eccentricity  $e_0$  and inclination  $i_0 = e_0/2$ . Most of our models have  $e_0$  independent of  $a_i$ ; some models have a constant initial horizontal velocity in each annulus. We consider moderately strong perturbations with  $e_0 = 0.01\text{--}0.06$ . Very close stellar flybys can produce  $e_0 \gtrsim 0.1$  (e.g., Ida et al. 2000; Kalas et al. 2000; Kobayashi & Ida 2001); our adopted  $e_0$  is 10–100 times larger than for a cold planetesimal disk, where  $e_0 \lesssim 10^{-3}$  (Kenyon & Luu 1999). We assume a power law variation of the initial surface density of solid material with heliocentric distance,  $\Sigma_i = \Sigma_0(a_i/a_0)^{-n}$ ; models with  $n = 1.5$  are ‘standard’.

We assume a stellar flyby instantaneously raises the orbital eccentricity and inclination of all planetesimals in the disk. Although not strictly accurate, this approximation is valid if the encounter between the passing star and the disk is short compared to the damping time. Any passing star that is not bound to the central star of the disk satisfies this requirement (Larwood 1997; Mouillet et al. 1997). A bound companion star with an orbital semi-major axis of  $\sim 1000$  AU or less can excite large planetesimal velocities over long timescales and may counteract damping. Embedded planets with radii of 500 km or larger can also counteract damping (Kenyon & Bromley 2001). We plan to consider both situations in future papers.

Our calculations follow the time evolution of the mass and velocity distributions of objects with a range of radii,  $r_{ik} = r_{min}$  to  $r_{ik} = r_{max}$ . The upper limit  $r_{max}$  is always larger than the largest object in each annulus. To save computer time, we do not consider small objects which do not affect significantly the dynamics and growth of larger objects. Usually this limit is  $r_{min} = 10$  cm. Erosive collisions produce objects with  $r_{ik} < r_{min}$ . These particles are ‘lost’ to the model grid. For most conditions, lost objects are more likely to be ground down into smaller objects than to collide with larger objects in the grid. Thus, our neglect of lost particles with  $r_{ik} < r_{min}$  is a reasonable approximation.

We do not consider planetesimals in the inner disk. Test calculations show that collisions damp particle velocities on short timescales,  $t_d \lesssim 10^3$  yr at  $a_i \lesssim 5$  AU. For a stellar flyby with an encounter velocity of 1–10 km s<sup>−1</sup>, these timescales are comparable to the duration of the flyby (see Larwood 1997; Mouillet et al. 1997). Our approximation of an instantaneous impulse to the disk is then invalid. The short damping timescales for the inner disk also suggest that the chances of finding a disk in this state are small. We therefore consider the evolution of the outer disk in these calculations.

For a cold disk of planetesimals with  $e_0 \lesssim 10^{-3}$ , the initial conditions of our calculations are sufficient to produce 1000 km or larger planets at 30 AU on timescales of  $\sim 10$  Myr for a minimum mass solar nebula (e.g., Stern & Colwell 1997a; Kenyon & Luu 1999; Kenyon et al. 1999). When a stellar flyby raises particle eccentricities by factors of 10–100, collisions between planetesimals promote erosion instead of growth by mergers. Our goal is to identify perturbations where collisional damping can reduce particle eccentricities and promote growth before erosive collisions reduce planetesimals to dust.

### 3. CALCULATIONS

#### 3.1. Cascades in Rings

To understand the response of a planetesimal disk to a stellar flyby, we begin by considering a small portion of a disk surrounding a 3 M<sub>⊙</sub> star. The ring consists of bodies with  $r_{min} = 10$  cm to  $r_{max}$  in 16 annuli with  $\delta a_i/a_i = 0.01$ . Each body has  $e_0 = 0.02$  and a mass density of 1.5 g cm<sup>−3</sup>. The mass spacing factor is  $\delta_1 = m_{k+1}/m_k = 2$  for all batches; the initial mass distribution has equal mass per batch. The surface density of solid material is  $\Sigma_d(a) = 0.15 x(a/35 \text{ AU})^{-3/2}$  g cm<sup>−2</sup>, where  $x$  is a dimensionless constant. Models with  $x = 1$ –2 have a total mass in solid material similar to the ‘minimum mass solar nebula’ at 2–20 AU (Weidenschilling 1977a; Hayashi 1981).

We calculate the collisional evolution for a set of models with  $x = 10^{-5}$  to 1 and  $r_{max} = 10$  m to 1000 km at  $a_{mid} = 35$  AU, 70 AU, and 140 AU. For computational speed, we adopt the Wetherill & Stewart (1993) fragmentation algorithm. Calculations with the Davis et al. (1985, 1994) algorithm evolve on a faster timescale when the collisional debris receives more kinetic energy per unit mass than the merged object (see Kenyon & Luu 1999). Collisional debris rarely has less kinetic energy per unit mass than the merged object (Davis et al. 1985, 1994). The fragmentation parameters for our standard models are  $Q_c = 5 \times 10^7$  erg g<sup>−1</sup> (crushing energy),  $S_0 = 2 \times 10^6$  erg g<sup>−1</sup> (impact strength), and  $V_f = 1$  m s<sup>−1</sup> (the minimum velocity for cratering).

Figures 1–2 outline the evolution of a model with  $x = 0.1$  and  $r_{max} = 10$  m at  $a_{mid} = 35$  AU. The 16 annuli in this standard model contain an initial mass of  $4 \times 10^{27}$  g ( $0.67 M_{\oplus}$ ). Erosive collisions dominate the early stages of this calculation. Collisions between small bodies with  $r_k =$

10–100 cm are completely disruptive; collisions between the largest bodies yield some growth and substantial cratering. Throughout the first  $10^4$  yr of the calculation, the initial ‘mass loss rate’ is large:  $\sim 10^{22}$  g yr $^{-1}$  is lost to particles with  $r_k < r_{min} = 10$  cm. This rate falls uniformly with time thereafter. Disruptive collisions between the ‘lost’ particles probably produce micron-sized grains which are ejected from the system on short timescales,  $\lesssim 10^5$  yr (e.g., Krivov et al. 2000).

As the calculation continues past  $10^4$  yr, collisional damping reduces the velocities of the mid-sized particles with  $r_k \sim 1$  m. Collisions between these and the largest bodies in the grid produce growth and some debris. The debris produced from these and other collisions flattens the cumulative number distribution from the initial  $N_C \propto m_i^{-1}$  to  $N_C \propto m_i^{-0.83}$ . For the rest of the calculation, the power law slope of the number distribution for the small bodies remains close to  $-0.83$  in each annulus. This slope is a standard result of coagulation when collisions produce debris (Dohnanyi 1969; Wetherill & Stewart 1993; Williams & Wetherill 1994; Tanaka et al. 1996; Kenyon & Luu 1999). As collisional damping continues to reduce the velocities of the mid-sized bodies, the largest bodies grow more rapidly. By  $t = 1$  Myr, the largest bodies have  $r_k = 25$  m (Figure 1, middle left panel). Although the largest and smallest bodies retain a large fraction of their initial eccentricities, the orbits of the mid-sized bodies are a factor of  $\sim 4$  less eccentric than their initial orbits (Figure 1; middle right panel). As growth proceeds, dynamical friction considerably reduces the velocities of the largest objects. Collisions damp the velocities of the smaller bodies. By  $t = 3$  Myr, the largest objects have  $r_k = 100$  m and most objects have  $e_k \leq 0.1 e_0$  (Figure 1, lower panels). From previous results, the largest bodies soon begin ‘runaway growth’ and reach sizes of 10–100 km or larger on timescales of  $\sim 30$ –100 Myr (Greenberg et al. 1978; Kenyon & Luu 1999; Kenyon et al. 1999). Because the production of debris – already below  $\sim 10^{21}$  g yr $^{-1}$  – drops rapidly during runaway growth, we stopped this calculation at  $t = 10$  Myr.

Figure 2 shows the time evolution of two ‘observables’, the radial optical depth and the fraction of stellar luminosity intercepted and reprocessed by solid material in the grid,  $L/L_\star$ . We follow Kenyon et al. (1999) and calculate the radial optical depth  $\tau_d$  of particles in the grid using the geometric optics limit. For particles with  $r_k < 10$  cm, we estimate a minimum optical depth  $\tau_{min}$  assuming Poynting-Robertson drag is efficient at removing the smallest objects and a maximum optical depth  $\tau_{max}$  assuming Poynting-Robertson drag removes none of the smallest objects. The dust luminosity follows directly from the solid angle of the dusty annulus as seen from the central star,  $L/L_\star = \tau H_d/a$ , where  $H_d$  is the scale height of the dust. The appendix describes our derivation of the radial optical depth and the reprocessed stellar luminosity in more detail (see also Krivov et al. 2000).

At  $t = 0$ , the optical depth is large because the dust production rate is large. The optical depth of the smallest grains,  $\tau_{min}$  and  $\tau_{max}$ , falls with the declining dust production rate and drops by  $\sim$  two orders of magnitude by  $t = 10$  Myr. For  $t < 1$  Myr, the optical depth of the mid-sized bodies grows with time. Collisional damping reduces the scale height of these particles, which increases their number density and thus their radial optical depth. By  $t = 10$  Myr, the largest bodies begin to grow rapidly and  $\tau_d$  falls back to its initial level. The optical depth continues to drop as runaway

growth concentrates more and more mass in the largest bodies.

The evolution of the dust luminosity depends on the evolution of the optical depth and the dust scale height<sup>2</sup> Because collisional damping reduces particle velocities throughout the calculation, the dust scale height falls monotonically with time. Unless the optical depth rises substantially, decreasing dust scale heights result in a declining dust luminosity. The small rise in  $\tau_d$  for  $t < 1$  Myr does not compensate for the decline in the scale height: the dust luminosity thus declines with time. At  $t = 0$ , the dust luminosity roughly equals the observed luminosities of debris disk systems with ring-like geometries,  $L/L_\star \sim 10^{-3}$  (e.g., Augereau et al. 1999b; Greaves et al. 1998; Jayawardhana et al. 1998; Koerner et al. 1998). By the end of the calculation, our most optimistic estimate of the dust luminosity falls below the smallest observed luminosity in known debris disk systems.

Although our predicted luminosities are close to those observed, the radial optical depths in our calculations,  $\sim 10^{-1}$  for the small particles and  $\sim 10^{-2}$  large particles in the grid, are significantly larger than values of  $\sim 10^{-3}$  or less typically quoted for debris disk systems. Published optical depths are usually derived from the ratios of the dust luminosity to the stellar luminosity and assume the dust is arranged in a spherical shell,  $L/L_\star = \tau(1 - \omega)$ , where  $\omega$  is the albedo. We adopt a more appropriate ring geometry; the dust luminosity is  $L/L_\star = \tau(1 - \omega)H/a$ . For rings with  $H/a \sim 0.01$ – $0.1$ , the radial optical depths must be  $\sim 10$ – $100$  times larger through the midplane of a ring than through a spherical shell. With this scaling, our optical depth estimates agree with published estimates for debris disk systems.

The luminosity evolution for each curve in Figure 2 is well-fit by a simple function

$$L/L_\star = \frac{L_0}{\alpha + (t/t_d)^\beta}, \quad (1)$$

where  $L_0$  is the initial dust luminosity. Because collisional damping reduces the eccentricities of the mid-sized particles by a factor of  $\sim 2$  at  $t = t_d$ , we call  $t_d$  the ‘damping time.’ At late times, the luminosity follows a power law with index  $\beta$ . We derive  $\beta = 1.35 \pm 0.02$  for the luminosity of small particles,  $L_{min}$  and  $L_{max}$ , and  $\beta = 1.05 \pm 0.02$  for the luminosity of large particles,  $L_d$ .

Calculations with other initial conditions produce similar results but on different timescales. High velocity collisions convert 25% or more of the initial mass into small particles ‘lost’ to the grid. Cratering produces most of the mass loss; catastrophic disruption is responsible for  $\lesssim 10\%$  of the lost mass. Collisional damping reduces the velocities of the mid-sized particles before cratering and catastrophic disruption convert all of the initial mass into debris. Because the collision lifetime

---

<sup>2</sup>We do not attempt to model the evolution of the dust luminosity during the stellar flyby. Because we assume a size distribution for small particles, the luminosity at  $t = 0$  in our models assumes that these particles reach the collisional size distribution,  $N_C \propto m_i^{-0.83}$ , instantaneously. In a more realistic calculation, the timescale to achieve this size distribution,  $\sim 10^4$  yr to  $10^5$  yr, is short compared to the damping time. Thus, our model provides a reasonably good approximation to the luminosity evolution following the flyby, but it makes no prediction for the change in  $L/L_0$  resulting from the flyby.

of a particle scales with the particle density, collisional damping is more effective in the more massive grids. Once the eccentricities of the mid-sized particles reach  $\sim 5 \times 10^{-3}$ , collisions begin to produce larger objects and less debris. Dynamical friction then reduces the velocities of the largest bodies, while collisional damping continues to ‘cool’ the mid-sized and smaller bodies. The most massive bodies eventually reach velocities small enough to initiate runaway growth, where the largest bodies grow rapidly and the mass loss rate is negligible (Kenyon & Luu 1999). We plan to describe runaway growth and the formation of planets in a future paper.

Figure 3 outlines the evolution of a model with  $x = 0.1$  and  $r_{max} = 10$  km at  $a_{mid} = 35$  AU. This model has fewer small particles than a grid with  $r_{max} = 10$  m; the smaller collision rate thus leads to a smaller luminosity and a smaller damping rate. The damping of the smallest particles is complete by  $t = 1$  Myr, but the largest particles still retain most of their initial eccentricities. Some of the largest particles grow from accretion of small bodies, but most remain at their original masses (Fig. 3, middle panels). Collisional damping continues until all of the debris-producing particles have small eccentricity at  $t = 4$  Myr. Despite their large eccentricities, the largest particles begin to grow rapidly (Fig. 3, lower panels). Dynamical friction then reduces their velocities over the next 10 Myr.

To compare these and other results as a function of the starting conditions, we derive the damping time  $t_d$  from least-squares fits to the luminosity evolution of each model. We use the maximum dust luminosity  $L_{max}$  for these fits. Unless Poynting-Robertson drag is efficient, the luminosity from small dust grains is larger than the luminosity contributed by larger objects in the main grid. The decline of the dust luminosity is therefore a convenient and relevant measure of the damping time. In most models, the dust luminosity declines by a factor of  $\sim 2$  at  $t = t_d$  and by a factor of  $\sim 20$  at  $t = 10t_d$ .

Figure 4 shows the variation of the damping time and maximum dust luminosity with  $x$  for models at 35, 70, and 140 AU. Models with the lowest surface densities are the least luminous and have the longest damping times. In systems with  $x < 10^{-3}$ , the damping time can exceed the stellar lifetime of  $\sim 1$  Gyr. For a given surface density, calculations with larger  $r_{max}$  have fewer small particles. These models therefore are less luminous and have longer damping times. Because the collision rate declines with distance from the central star, the luminosity also declines with increasing  $a_{mid}$ . These results indicate that particle collisions in rings with  $x > 10^{-2}$  can produce dust luminosities similar to those observed in a real debris disk system with a ring geometry. Collisional damping reduces these luminosities by an order of magnitude on timescales of 100 Myr or less.

To test the sensitivity of  $L_d$  and  $t_d$  to other initial conditions, we vary the initial eccentricity  $e_0$ , the minimum and maximum particle size in the grid ( $r_{min}$  and  $r_{max}$ ); the slope  $\gamma$  of the initial mass distribution,  $N_C(m) \propto m^{-\gamma}$ ; the fragmentation parameters  $Q_c$  and  $S_0$ ; and the mass density of the particles  $\rho_{ik}$  for calculations at  $a_{mid} = 35, 70$ , and 140 AU. Because the dust luminosity is proportional to the collision rate, models with larger numbers of small particles are more luminous



than models with fewer small particles. These models also damp more rapidly. Thus, models with  $\gamma > 1$  and  $r_{min} < 10$  cm are more luminous and damp more rapidly than models with  $\gamma < 1$  and  $r_{min} > 10$  cm. Models with ‘weaker’ bodies – smaller  $Q_c$  and  $S_0$  – or with larger, less dense bodies are also more luminous and damp more rapidly. These models yield a simple relation between the damping time and the luminosity of bodies in the grid at  $t = 0$ :

$$\log (t_d \cdot L_{d,0}/L_\star) \approx 0.4 + 1.33 \log (a_{mid}/35 \text{ AU}) . \quad (2)$$

The maximum dust luminosity at  $t = 0$  is

$$\log (t_d \cdot L_{max,0}/L_\star) \approx 2.1 + 1.33 \log (a_{mid}/35 \text{ AU}) . \quad (3)$$

The scatter in the coefficients is  $\pm 0.1$  for a wide range of initial conditions. At late times, the dust luminosity follows a power law,

$$\log L_{max}/L_\star \propto (t/t_d)^{-1.33 \pm 0.05} . \quad (4)$$

For the luminosity evolution of the particles in the main grid, we derive

$$\log L_d/L_\star \propto (t/t_d)^{-1.0 \pm 0.1} . \quad (5)$$

We identify only two exceptions to these relations. In calculations with large  $e_0$  or weak bodies, collisions can remove most of the initial mass on timescales shorter than the relevant damping time. Figure 5 shows the ratio of final mass in the ring  $M_f$  to the initial mass  $M_i$  as a function of  $e_0$  for planetesimals with  $S_0 = 2 \times 10^6 \text{ erg g}^{-1}$ . For modest perturbations with  $e_0 \lesssim 0.03$  ( $a_i/35 \text{ AU}$ )<sup>1/2</sup>, collisions damp particle velocities before the ring loses a significant amount of mass to small particles with  $r_i < r_{min}$ . These models follow the  $L_d - t_d$  relations. For strong perturbations with  $e_0 \gtrsim 0.04$ – $0.06$  ( $a_i/35 \text{ AU}$ )<sup>1/2</sup>, erosion removes a significant amount of mass from the ring before damping reduces particle velocities. These models have 25%–50% longer damping times; the asymptotic decline of the luminosity is identical to models with smaller perturbations,  $L_d \propto t^{-1}$  for the large particles and  $L_{max} \propto t^{-1.33}$  for the small particles.

In calculations with very large bodies ( $r_{max} \gtrsim 500$  km), viscous stirring and dynamical friction by the largest bodies in the grid can counteract collisional damping. The dust luminosity can then remain large for timescales of  $\sim 100$  Myr or longer. Because collisional cascades in rings with embedded planets – and no stellar flyby – behave in a similar fashion, we plan to consider these models in more detail in a separate paper.

### 3.2. Cascades with Gas and Poynting-Robertson Drag

Gas drag can be an important factor in planetesimal evolution (e.g., Nakagawa et al. 1983; Wetherill & Stewart 1993). Interactions between solid bodies and the gas damp particle velocities

and remove particles from the model grid. Both processes scale with the local gas density,  $\rho_{g,i}$ . To understand how these processes affect the dust luminosity and the damping time, we calculated a set of ring models for different initial values of the gas-to-dust mass ratio,  $X_g \equiv \Sigma_g/\Sigma_d$ . The interstellar medium has  $X_g = 100$ ; observed limits in debris disk systems are uncertain (Zuckerman et al. 1995; Dent et al. 1995; Lecavelier des Etangs et al. 1998; Greaves, Coulson, & Holland 2000a; Thi et al. 2001). The appendix summarizes our treatment of particle removal and velocity damping. We held the gas density fixed with time;  $X_g$  therefore increases with time as fragmentation and gas drag remove solid bodies from the grid. Calculations with  $X_g = 1$  are indistinguishable from models without gas. Gas drag modifies the evolution of solid bodies for  $X_g \gtrsim 10$ . The following paragraphs describe the evolution for  $X_g = 10$  and  $X_g = 100$ .

Figure 6 shows the mass and velocity distributions at several times during the evolution of a model with  $X_g = 10$ . The initial conditions are identical to the model of Figure 1: small bodies with  $r_{min} = 10$  cm to 10 m have the same initial eccentricity,  $e_0 = 0.02$ , and a total mass of  $0.67 M_\oplus$ , in 16 annuli at  $a_{mid} = 35$  AU from a central  $3 M_\odot$  star. Interactions between solid particles and the gas have a modest impact on the evolution of this model. After 1 Myr, gas drag has swept less than 0.01% of the initial mass through the innermost annulus and out of the grid. Compared to a model without gas drag, orbital eccentricities are  $\sim 5\%$  to  $10\%$  smaller and the largest bodies are  $\sim 10\%$  to  $20\%$  larger (Figure 6, middle panels). The amount of mass lost to small particles is  $\sim 24\%$ , compared to  $\sim 25\%$  in a model without gas drag. After 3 Myr, gas drag is responsible for only  $\sim 0.02\%$  of the total mass loss. Orbital eccentricities are now  $\sim 20\%$  smaller, and the largest bodies are  $\sim 40\%$  larger (Figure 6, lower panels). This model reaches runaway growth earlier than a model without gas drag; the final mass distributions of models with and without gas drag are indistinguishable (Kenyon & Luu 1999).

Interactions between solid bodies and the gas are much more important when  $X_g = 100$  (Figure 7). After 0.5 Myr, gas drag reduces orbital eccentricities of the smallest bodies by a factor of four, and the largest bodies begin to grow by mergers (Figure 7, middle panels). The mass lost from gas drag is small,  $\sim 0.1\%$  of the initial mass, compared to the mass lost from erosive collisions,  $\sim 22.5\%$ . By 1 Myr, gas drag, dynamical friction, and collisional damping cool the small bodies well before the largest objects grow to sizes of 100 m (Figure 7, lower panels). The small orbital eccentricities of this model yield an early runaway growth phase and the production of several Pluto-sized objects on timescales of 10–30 Myr (Kenyon & Luu 1999). The mass of this model at 1–3 Myr is  $\sim 3\%$  larger than models without gas drag at similar phases; this difference does not yield significantly larger objects after 10–30 Myr compared to models without gas drag.

Despite their more rapid evolution, models with gas drag follow nearly the same luminosity-damping time relation as models without gas drag. We derive  $\log(t_d \cdot L_{max,0}) = C + 1.33 \log(a_{mid}/35 \text{ AU})$  for these models. Damping is more efficient when gas drag is important; larger gas-to-dust ratios imply smaller values of  $C$ . Thus, the damping times derived from models without gas drag are upper limits to the lifetime of a collisional cascade produced by a stellar fly-by. We also derive the same power-law decline of dust luminosity with time,  $\log L_{max}/L_\star \propto (t/t_d)^{-1.33}$ , as

in models without gas drag.

To complete this portion of our study, we consider mass loss from Poynting-Robertson drag for various values of the stellar luminosity and the particle mass density. Mass loss from Poynting-Robertson drag is less than 1% of losses from fragmentation and gas drag unless the stellar luminosity exceeds  $100 L_{\odot}$  ( $\rho_m/1.5 \text{ g cm}^{-3}$ ). Damping of the horizontal velocity is also negligible. For A-type stars with  $L_{\star} \lesssim 100 L_{\odot}$ , Poynting-Robertson drag does not modify our conclusions unless the mass density of the mid-sized bodies is much smaller than  $1 \text{ g cm}^{-3}$ . Calculations with low density bodies yield smaller damping times than implied by equations (1) and (2). Although Poynting-Robertson drag generally is not important for the large grains considered here, removal of smaller grains can modify the optical depth (see the appendix). We plan to investigate this possibility in a future study.

### 3.3. Cascades in Disks

The ring calculations in §3.1 and §3.2 yield several interesting conclusions about collisional cascades in planetesimal disks. Stellar flybys can produce long-lived cascades in low mass disks, but the dust luminosity produced in these cascades is small,  $L_{max}/L_{\star} \lesssim 10^{-5}$  for  $x \lesssim 10^{-2}$ . Cascades in rings with 1% or more of the minimum mass solar nebula produce larger dust luminosities but have short observable lifetimes. The damping times in these models are  $\sim 1\text{--}10$  Myr. These timescales are short compared to the ages of the oldest debris disk systems,  $\sim 100\text{--}500$  Myr (Habing et al. 1999; Song et al. 2000a; Spangler et al. 2001).

To test these conclusions in more detail, we consider more complete disk models. The disk consists of 64 annuli with  $\Delta a_i/a_i = 0.025$  and extends from  $a_{in} = 30$  AU to  $a_{out} = 150$  AU. As in §3.1, the disk contains bodies with  $r_{min} = 10$  cm to  $r_{max}$  and a mass density of  $1.5 \text{ g cm}^{-3}$ . All of the bodies have the same horizontal velocity with respect to a circular orbit; the initial eccentricity in each annulus is  $e_i = e_1 a_i^{1/2}$  where  $e_1$  is the eccentricity in the innermost annulus. This condition yields a constant initial horizontal velocity in the disk. The mass spacing factor is  $\delta_1 = m_{k+1}/m_k = 2$  for all batches; the initial mass distribution has equal mass per batch. We adopt the Wetherill & Stewart (1993) fragmentation algorithm with  $Q_c = 5 \times 10^7 \text{ erg g}^{-1}$ ,  $S_0 = 2 \times 10^6 \text{ erg g}^{-1}$ , and  $V_f = 1 \text{ m s}^{-1}$ .

Figures 8–12 outline the evolution of a model with  $x = 0.1$ ,  $r_{max} = 10$  m, and  $e_1 = 0.02$ . The initial surface density is  $\Sigma_i = 3 \text{ g cm}^{-2} (a_i/1 \text{ AU})^{-3/2}$ ; the initial mass in solid material is  $10 M_{\oplus}$ . At the inner edge of the disk, collisions rapidly damp orbital eccentricities on timescales of 1 Myr or less. The largest bodies double their radius in the first 1 Myr and quadruple their radius in the first 10 Myr. Because collision cross-sections scale with disk radius as  $A \propto a_i^{-3}$ , collisional damping proceeds very slowly at the outer edge of the disk. Growth is slow. Collisional damping starts to affect mid-sized bodies in the outer disk at 1 Myr, when bodies at  $a_i \lesssim 40$  AU are completely damped and starting to grow rapidly (Figure 8; middle panels). Gravitational focusing leads to

faster growth once mergers dominate erosive collisions. Thus, large bodies at 30 AU have entered the runaway growth phase when 10 cm bodies at 150 AU are just starting to grow (Figure 8; lower panels).

Figure 9 shows the sensitivity of collisional damping and of the growth rate of the largest objects to position in the disk. The initial eccentricities of the smallest particles follow a power-law,  $e_i \propto a_i^{1/2}$ ; the scale height of these bodies above the disk midplane is thus  $H \propto a_i^{3/2}$ . The eccentricity of the smallest particles in the grid damps by a factor of  $\sim 2$  at  $a_i = 30$  AU in 1 Myr, when small particles at the outer edge of the grid have almost all of their initial orbital eccentricity. At 10 Myr, damping has reduced the orbital eccentricities of all small particles by factors of 2 or more. The eccentricities of the smallest particles then vary with disk radius as  $e_i \propto a_i^{0.85}$ . The power-law slope of this relation falls to 0.8 at 50 Myr. This behavior yields a very steep variation of the scale-height with radius,  $H \propto a_i^{1.8}$ .

The merger rate is more sensitive to disk radius. For  $t < 10$  Myr, growth rates are linear, because gravitational focusing factors are small. The radius of the largest body is a smooth function of disk radius,  $r_{i,max} \propto a_i^{-\gamma}$  with  $\gamma \gtrsim 1.5$ . Once particles in the inner disk reach sizes of  $\sim 1$  km, gravitational focusing factors increase and growth becomes non-linear. Annuli in the runaway growth phase depart from a smooth power-law variation of  $r_{i,max}$  with  $a_i$ , as indicated by the sharp rise in  $r_{i,max}$  for  $a_i \lesssim 40$  AU at 50 Myr.

The total dust luminosity of this model follows the evolution derived for the ring models in §3.1 (Figure 10). At  $t = 0$ , the maximum dust luminosity of  $L_{max}/L_\star \sim 6 \times 10^{-3}$  is comparable to luminosities observed in  $\beta$  Pic and other luminous debris disk systems (Augereau et al. 1999a; Barrado y Navascués et al. 1999; Habing et al. 1999; Song et al. 2000b). The dust luminosity decreases with time and reaches  $L_{max}/L_\star \sim 2 \times 10^{-5}$  at  $t = 50$  Myr. This luminosity is close to luminosities observed in  $\alpha$  Lyr and other faint debris disk systems (Kalas 1998; Spangler et al. 2001). Equation (1) describes the time-evolution of the luminosity remarkably well. The luminosity-damping time relation is

$$\log t_d \cdot L_{max,0}/L_\star = 3.16 \pm 0.05. \quad (6)$$

At late times,

$$L_{max}/L_\star \approx 4 \times 10^{-3} (t/t_d)^{-1.03 \pm 0.02}. \quad (7)$$

Kalas (1998) derives  $L \propto t^{-1}$  for known debris disk systems with reliable ages.

To visualize the time evolution of the luminosity for this disk model, we assume a pole-on system where each annulus in the grid has a dust opacity derived in the geometric optics limit from the number density (§A.6). The luminosity per unit surface area radiated by each annulus is then a simple function of the opacity and the dust scale height (Kenyon et al. 1999). We adopt the scale height for the smallest particles in the grid. This procedure yields the bolometric surface brightness. If the particle albedo is large and independent of grain size, the predicted surface brightness should be close to the optical or near-IR surface brightness of scattered light.

Figure 11 shows how the radial surface brightness profile changes with time. At the start of our calculations, models with a power-law surface density distribution  $\Sigma_i$  produce a power-law surface brightness distribution  $I_i$ . For  $\Sigma_i \propto a_i^{-3/2}$ , we derive  $I_i \propto a_i^{-7/2}$ . For  $t \lesssim 1$  Myr, collisions damp particle eccentricities in the inner disk,  $r_i \sim 30\text{--}60$  AU. Smaller collision velocities produce less dust; the surface brightness fades. At  $t = 1$  Myr, the surface brightness is nearly constant for  $r_i = 30\text{--}60$  AU and gradually approaches the initial  $I_i \propto a_i^{-7/2}$  at  $r_i \gtrsim 100$  AU. As the calculation proceeds, collisions damp particle velocities in the outer disk. After  $t \approx 10$  Myr, the surface brightness in the inner disk declines by nearly two orders of magnitude; the outer disk fades by  $\sim 30\%$ . All of the disk then fades by roughly an order of magnitude over the next 20–40 Myr. When we terminate the calculation at 50 Myr, the surface brightness distribution is much more shallow than the initial distribution, with  $I_i \propto a_i^{-1/2}$  instead of  $I_i \propto a_i^{-7/2}$ .

Figure 11 illustrates how coagulation concentrates mass into large objects with small optical depth. At 50 Myr, the radial gradient in the surface density of solid material is similar to the initial gradient, with  $\Sigma \propto a_i^{-1.55}$ . Because material in the inner disk has more frequent collisions than material in the outer disk, the inner disk has more material in large objects with  $r_i \gtrsim 100$  m than the outer disk. The surface density of small objects thus grows with radius; for  $t \gtrsim 10$  Myr,  $\Sigma_{small} \propto a_i^{1.5}$  for  $r_i \lesssim 10$  cm. There is some evidence for this behavior in real systems: the particle disks in BD+31°643 (Kalas & Jewitt 1997) and HD 141569 (Weinberger et al. 1999) have regions where the number density of small particles appears to increase in radius. We plan additional calculations to see if this feature of the calculations is characteristic of flyby models or all planet-forming particle disks.

Figure 12 shows disk images at six times in the evolutionary sequence. An animation of the disk evolution is available in the electronic version of this paper. To construct predicted images from the surface brightness profiles, we assume a simple power law relation to convert surface brightness to pixel intensity. We simulate an observation by adding counting noise to the intensity of each pixel, but we do not convolve the image with a ‘seeing disk.’ These approximations ignore radiative transfer effects in the disk and the variation of disk flux with wavelength, but the resulting images accurately illustrate the physical behavior of the dust luminosity with time.

To investigate the sensitivity of these results to the starting conditions, we consider several models with different values for  $e_1$  and  $x$  and several models with gas drag. Full disk models require more computer time than ring models; this study is therefore more limited than the parameter study of §3.1. As long as erosive collisions do not exhaust the supply of mid-sized bodies before collisional damping can reduce particle eccentricities, models without gas and Poynting-Robertson drag yield the luminosity-damping time relation in equation (6) to an accuracy of 10% or better independent of the initial conditions. Low mass disks are less luminous and longer lived than massive disks. Calculations with gas drag ( $X_g = 100$ ) evolve  $\sim 30\%$  faster than models without gas drag. Equation (5) thus provides an upper limit to the damping time for a disk with initial luminosity  $L_{max,0}/L_\star$ .

The evolution of the scale height is the main difference between models with and without gas

drag. When the gas density is low ( $X_d \lesssim 1\text{--}3$ ), gas drag does not reduce significantly the orbital eccentricities of the smallest particles in the grid. Collisional damping and dynamical friction dominate the velocity evolution; the scale height of small particles exceeds the scale height of large particles. When the gas density is larger ( $X_d \gtrsim 10$ ), the small particles are more closely coupled to the gas and have more circular orbits. The mid-sized particles then have the largest scale heights. If the gas and small particles are well-mixed perpendicular to the disk midplane, the dust has a large scale height and a large dust luminosity (Kenyon & Hartmann 1987). If mixing between dust and gas is poor, small dust particles settle to the midplane; the dust luminosity is then small. Detailed hydrodynamical calculations are necessary to derive the outcome of a collisional cascade in a planetesimal disk with large amounts of gas.

Full disk calculations yield the same behavior with initial eccentricity as ring models. For annuli with  $e_0 \lesssim 0.05 (a_i/35 \text{ AU})^{1/2}$ , collisional damping reduces particle velocities before the disk loses more than half of its initial mass. The disk loses more than 95% of its initial mass for strong perturbations with  $e_0 \gtrsim 0.05 (a_i/35 \text{ AU})^{1/2}$ . In these strong perturbations, collisional damping reduces particle velocities sufficiently to allow growth by mergers and the formation of 1 km or larger bodies. The timescale for planet formation is then very long,  $\sim 1$  Gyr or longer.

Our results indicate that complete disk models evolve on faster timescales than ring models (see also Kenyon & Bromley 2001). In ring models, planetesimals at the edges of the grid interact with fewer annuli than planetesimals in the middle of the grid. Collisional damping is less effective with fewer collisions. Partial disk models thus damp more slowly and lose more mass than complete disk models. At 35 AU, complete disk models lose  $\sim 20\%$  less mass than ring models. This difference rises to  $\sim 50\%$  at 140 AU. More effective damping and less mass loss yield larger bodies on shorter timescales in complete disk models.

### 3.4. Limitations of the Models

Statistical simulations of planetesimal growth in a dusty disk have a long history, with well-known limitations and uncertainties (Wetherill 1980; Greenberg et al. 1984; Davis et al. 1985; Barge & Pellat 1991; Spaute et al. 1991; Lissauer & Stewart 1993; Wetherill & Stewart 1993; Stern & Colwell 1997a; Weidenschilling et al. 1997; Kenyon & Luu 1998; Inaba et al. 2001). The particle-in-a-box formalism assumes a homogeneous spatial distribution of solid bodies with small velocities relative to the local circular velocity. This assumption is good until runaway growth produces a few massive bodies not distributed uniformly in space (Kokubo & Ida 1996). Our simulations never reach this limit. Our calculations also require a specific algorithm for collision outcomes (§2 and the appendix). As long as particle collisions produce damping and some debris, our derived relations for the evolution of luminosity as a function of initial disk mass are remarkably independent of the details of the collision algorithm. The collisional damping prescription is more important; changing the coefficients in the algorithm (equations A8 and A9 of the appendix) changes the damping times by a similar factor. We have not investigated the sensitivity of the results to

the form of the damping equations. We have tested our prescription for velocity evolution in the low velocity limit, where the relative collision velocity is small compared to the Hill velocity (Barge & Pellat 1990; Wetherill & Stewart 1993; Kenyon & Luu 1998; Stewart & Ida 2000; Kenyon & Bromley 2001). The statistical approach is invalid in this limit. Ida (1990), Barge & Pellat (1990), Ida & Makino (1992, 1993), and Wetherill & Stewart (1993) have described solutions to this problem; we use the Ida & Makino (1992) approach. Tests with other approaches yield the same results.

The implementation of the algorithms produces other limitations. Our multiannulus calculations eliminate many of the constraints associated with calculations of a single accumulation zone (Wetherill 1990b; Wetherill & Stewart 1993; Weidenschilling et al. 1997; Kenyon & Luu 1999). We can treat collisions and gravitational perturbations between particles in adjacent annuli, and the drift of particles through adjacent annuli due to gas drag and Poynting-Robertson drag. The current calculations do not include algorithms for orbital migration of planetesimals or the evolution of gas in the disk (including gas accretion), but these processes are not important for the situations we investigate here.

Uncertainties resulting from the finite mass and spatial resolution should be small. Calculations with coarse mass resolution within an annulus lag higher resolution simulations by 10% to 20% but yield nearly the same mass and velocity distributions (see Kenyon & Luu 1998, 1999). Calculations with finer spatial resolution are indistinguishable from the simulations described above at the 5% level. These differences grow with the mass of the largest object in the grid but are not important for the relatively small mass objects we consider here.

To compute the dust luminosity, we assume two limits to the dust opacity of small objects. We make these assumptions to avoid computing the time evolution of small particles, which have a negligible impact on the evolution of larger planetesimals in the grid. In most planetesimal disks, the large opacity limit is appropriate, because the timescales for Poynting-Robertson drag are  $\sim 1$  Myr or longer at 30 AU and  $\sim 25$  Myr or longer at 150 AU. These timescales are long compared to the damping times of massive, luminous planetesimal disks. For more luminous central stars with  $L_\star \sim 100 L_\odot$ , the small opacity limit is appropriate, because Poynting-Robertson drag can remove small grains on timescales much shorter than 1 Myr at 30 AU. We plan to address these uncertainties in more detail in a future paper.

In our complete disk models, we adopt a shallow variation of the initial eccentricity of planetesimals with disk radius,  $e_0 \propto a_i^{1/2}$ . The ratio of the initial horizontal velocity to the shattering velocity of a dust grain is then independent of  $a_i$ , which allows us to investigate collisional damping without worrying about the importance of different fragmentation algorithms. This approximation is reasonable for moderately strong perturbations where the passing star has a periastron of  $\sim 600$  AU. Closer stellar flybys produce stronger perturbations with  $e_0 \propto a_i^{5/2}$  (Ida et al. 2000; Kalas et al. 2000; Kobayashi & Ida 2001). In a strong perturbation, planetesimals in the outer disk are depleted more rapidly than those in the inner disk. Even if the outer disk loses nearly all of

its initial mass, our calculations indicate that collisional damping should reduce particle velocities and allow planet formation on long timescales. We plan to investigate this possibility in a future paper.

The speed of the computer is a final limitation to these calculations. Although larger test simulations are possible, practical considerations limit calculations of model grids to 64–128 annuli. For reasonable spatial resolution, the maximum extent of our grid is a factor of 5–10 in distance from the central star. We are thus 1–2 orders of magnitude from constructing model grids of complete solar systems. For a given set of algorithms, the timescales and dust luminosities derived here should be within 10% to 50% of those derived from more extensive models. Limitations on the extent of the radial grid are more important for addressing the interfaces between (i) gas giants and terrestrial planets and (ii) gas giants and the Kuiper Belt in our solar system. Similar problems occur in evolutionary calculations of other types of circumstellar disks. Faster computers should resolve these difficulties in the next few years.

#### 4. DISCUSSION AND SUMMARY

Stellar flybys can plausibly produce collisional cascades in a planetesimal disk. When the mass of solid material in the disk is 1% or more of the minimum mass solar nebula ( $\sim 1\text{--}100 M_{\oplus}$  of solid material at 30–150 AU), flybys which increase planetesimal velocities close to the shattering limit can produce dust luminosities similar to those observed in known debris disk systems. The dust luminosity correlates with the disk mass. Collisional damping in these disks is very efficient; dust production decreases dramatically on timescales of 1 Myr or less. The most luminous and most massive disks damp the fastest. These conclusions are independent of many uncertainties in the calculations, including the initial mass distribution, the fragmentation parameters, and the mass density of planetesimals.

Our calculations indicate two outcomes for a collisional cascade induced by a moderately close stellar flyby. If the flyby produces relative velocities which exceed the strength of a planetesimal, disruptive collisions nearly exhaust the supply of planetesimals before collisional damping becomes effective. Most planetesimals are eventually ground to dust and planet formation is difficult (see also Kobayashi & Ida 2001). For icy planetesimals with  $S_0 = 2 \times 10^6 \text{ erg g}^{-1}$ , this limit is  $e_0 \gtrsim 0.05 (a_i/35 \text{ AU})^{1/2}$ .

When a flyby produces a smaller perturbation in the disk, collisional damping reduces planetesimal velocities on relatively short timescales. This process allows the disk to retain a significant mass in large planetesimals, which collide and merge to form planets. Our ability to detect the collisional cascade observationally depends on the disk mass. Collisional cascades in disks with  $\sim 1\%$  or more of the minimum mass solar nebula produce dust luminosities,  $L_{\text{max}}/L_{\star} \gtrsim 10^{-5}$ , comparable to those observed in debris disk systems (Kalas 1998; Spangler et al. 2001).

Collisional damping is a new feature in models of the evolution of collisional cascades in



planetesimal disks. Previous models assumed that collisions preserve the eccentricity and inclination distributions of planetesimals in the disk (e.g., Mouillet et al. 1997; Augereau et al. 2001, see also Artymowicz 1997, Lagrange et al. 2000, and references therein). Dust grains produced by collisions thus had the same orbits as their progenitors. In our models, ‘collisionless’ systems with long collision timescales yield optical depths and dust luminosities much smaller than those observed (Figures 4 and 10). Systems with larger optical depths and dust luminosities have short collision times and short damping timescales. This conclusion is an extension of earlier work on the debris disk system HR 4796A and the Kuiper Belt in our solar system, where disks with masses of solid material comparable to or larger than the minimum mass solar nebula allow the growth of Pluto-sized objects, which stir the velocities of smaller objects to the shattering velocity and produce observable collisional cascades (Kenyon & Luu 1999; Kenyon et al. 1999, see also Stern & Colwell 1997a,b).

Following a flyby, equation (1) fits the evolution of the dust luminosity to remarkably high accuracy. Because damping and dust production depend on the collision rate, collision physics sets the form of this relation. To derive the limiting form of equation (1), we assume an ensemble of identical planetesimals. The coagulation equation is  $dn/dt \propto n^2$  (§A.2). The dust production rate is  $dm/dt \propto m^2 n^2 \propto n^2$  where  $m$  is the mass of a planetesimal. Thus, the disk mass and the number density of planetesimals fall with time,  $M_d \propto t^{-1}$ . Because the disk has constant surface area, the surface density follows the same relation,  $\Sigma \propto t^{-1}$ . The left panels of Figure 3 verify this relation for the damping time,  $t_d \propto \Sigma_d^{-1}$ . The luminosity of the planetesimals is proportional to the disk mass, which yields  $L \propto t^{-1}$ ; our models follow this relation faithfully (Figure 2 and 10). The dust luminosity depends on the mass distribution of planetesimals for  $r_k < r_{min}$ , where  $r_{min}$  is the minimum planetesimal radius in the grid. The appendix describes two limits on this mass distribution. The maximum dust mass assumes that Poynting-Robertson and other drag forces do not remove particles from the grid; the minimum dust mass assumes that drag forces remove particles efficiently from the grid. In both limits, the dust mass is proportional to the disk mass (Figure 3, right panels). The dust luminosity thus declines with time,

$$L_{max,min} \propto t^{-1}. \quad (8)$$

Kalas (1998) derives the same relation from observations of debris disks. Our detailed models for complete disks yield this relation; because planetesimals have fewer annuli to interact with, the relation for ring models is steeper.

Spangler et al. (2001) derive a different relation for the time-variation of luminosity in a collisional cascade,  $L_d \propto t^{-2}$ . They assume that the dust clearing time is shorter than the age of the system and conclude that the dust luminosity is proportional to the instantaneous dust production rate,  $dn/dt$ . However, the dust luminosity is proportional to  $dn/dt$  only if planetesimal collisions produce dust which escapes the system on timescales shorter than the collision time. Because Poynting-Robertson drag and gas drag are slow processes in the outer disk, radiation pressure is

the only mechanism capable of removing particles from a large debris disk on short timescales<sup>3</sup>. Particles with sizes of 10  $\mu\text{m}$  or larger are unaffected by radiation pressure. Planetesimal collisions thus build up a reservoir of dust grains with sizes of 10  $\mu\text{m}$  or larger, while radiation pressure ejects smaller grains (Burns, Lamy, & Soter 1979; Backman & Paresce 1993; Artymowicz 1997). For the power law cumulative mass distribution appropriate for collision debris,  $N_C(m) \propto m^{-0.83}$  (Dohnanyi 1969; Davis et al. 1985; Wetherill & Stewart 1993; Kenyon & Luu 1999), the optical depth of grains ejected by radiation pressure is a factor of 10 or more smaller than the optical depth of larger grains. The larger grains in an annulus thus make a larger contribution to the dust luminosity than smaller grains accelerated away from the annulus. The decline of the dust luminosity then depends on the rate of decline for the total disk mass,  $L_{\text{max}} \propto M_d \propto t^{-1}$ .

Our results suggest modifications of the picture for the formation and early evolution of the Kuiper Belt. Ida et al. (2000) propose a stellar flyby to explain the structure of the outer Kuiper Belt in our solar system. In their model, a stellar encounter with a distance of closest approach of  $\sim 100$  AU excites the large orbital eccentricities and inclinations observed for 50–500 km objects at distances of 30–50 AU from the Sun. Collisions between these objects lead to a collisional cascade which erodes the mass of the inner Kuiper Belt over time. In our calculations, collisional damping of 1–100 m planetesimals accompanies mass erosion; dynamical friction then damps the eccentricities and inclinations of the largest objects on short timescales,  $\sim 1$ –10 Myr for a minimum mass solar nebula model and  $\sim 100$  Myr for a disk with a mass of solid material equal to the mass of the current Kuiper Belt. Our models predict damping times of 5 Gyr or longer only when the disk has a small mass in solid objects with radii of 1 km or less. Coagulation models which can produce 50–500 km Kuiper Belt objects at 30–40 AU leave most of the initial mass in smaller objects with radii of 0.1–10 km (Kenyon 2002; Kenyon & Luu 1999, see also Stern & Colwell 1997a,b). Thus, if a stellar encounter is responsible for the large orbital eccentricities observed in Kuiper Belt objects, our models suggest that this encounter occurred after some other process depleted the Kuiper Belt of 0.1–1 km objects. We plan to investigate the idea that stirring by one or more Pluto-sized objects embedded in the Kuiper Belt can explain this depletion.

Kalas & Jewitt (1995, see also Kalas et al. 2000; Kalas, Deltorn, & Larwood 2001; Larwood & Kalas 2001) propose a stellar flyby model to explain structures observed in the  $\beta$  Pic debris disk. In their picture, a recent,  $\sim 10^5$  yr, stellar encounter produces an asymmetric ring system and other dynamical features in the disk (Kalas et al. 2000). The highly perturbed orbits of planetesimals in the disk lead to a collisional cascade and copious dust production. Although we cannot calculate planetesimal evolution in the  $\sim 1000$  AU  $\beta$  Pic disk with adequate spatial resolution, our 30–150 AU disk model in §3.3 provides a reasonable first approximation to the evolution of a collisional cascade induced by a moderately close stellar flyby in the inner portion of a large disk. The maximum dust

---

<sup>3</sup>Poynting-Robertson and gas drag can efficiently remove small particles from a planetesimal disk at distances of 1–5 AU from the central star. Relatively rapid dust removal might account for the large inner ‘holes’ observed in some debris disk systems (see also Backman & Paresce 1993; Artymowicz 1997; Koerner et al. 1998; Lagrange et al. 2000).

luminosity of  $L_{max,0}/L_{\star} \sim 4 \times 10^{-3}$  is close to the bolometric luminosity ratio  $L_b/L_{\star} \sim 3 \times 10^{-3}$  observed in  $\beta$  Pic (Backman & Paresce 1993). The damping time of the model,  $\sim 3 \times 10^5$  yr, indicates that collisions do not wash out either the observed ring structure or the radial variation of eccentricity and inclination at distances of 100–1000 AU on timescales similar to the apparent dynamical age of  $\sim 10^5$  yr. However, our models produce significant collisional damping at 30–50 AU on short timescales. Damping produces an apparent hole in the disk, with smaller dust production than annuli in the outer disk (Figures 11–12). In principle, our models can produce changes in the slope of the radial surface brightness distribution similar to that observed in the  $\beta$  Pic disk (Golimowski, Durrance, & Clampin 1993; Augereau et al. 2001). Radiative transfer calculations similar to those of Kenyon et al. (1999) will allow us to make a detailed comparison between our models and observations.

Associating stellar flybys with other debris disk systems seems less practical. The damping time-luminosity relation (equation (6)) implies that all collisional cascades induced by stellar flybys have luminosities which decline below  $L_{max}/L_{\star} \sim 10^{-5}$  on timescales of 100 Myr or less. Source statistics suggests that nearly all stars are born with a disk (Lada 1999); many main sequence stars also have disks (Habing et al. 2001). Several known debris disk systems have ages of 500 Myr or more (Song et al. 2000b; Spangler et al. 2001). Recent flybys for all objects are unlikely; the chance probability of a stellar encounter which passes within  $\sim 500$  AU of a nearby field star is 1% or less in  $\sim 100$  Myr (Frogel & Gould 1998; Garcia-Sánchez et al. 1999). We suspect that stirring by embedded planets or a binary companion induces collisional cascades in most debris disk systems. We plan future papers to address this issue.

Our results suggest caution when interpreting observed relations between dust luminosity and age in debris disk systems. Most evolutionary processes in a planetesimal disk scale with the orbital period. The factor of 4–6 range in the stellar mass among known debris disk systems implies a range of 2–2.5 in evolutionary timescales for systems with the same initial disk mass and disk radius. In an ensemble of stars with a range of temperatures and luminosities, Poynting-Robertson drag will cause lower dust luminosities in disks with luminous stars compared to less luminous stars. Poynting-Robertson and gas drag may also reduce disk luminosities below current detection limits on shorter timescales for luminous stars than for less luminous stars. This behavior suggests that the timescale for disk evolution should correlate with the nature of the central star. Song et al. (2000b) comment on this effect in their data for 10–15 debris disk systems. Although the trend described by Song et al. (2000b) is encouraging, current samples are too small and the selection effects too uncertain to make robust statements about timescales for disk evolution. Larger samples with smaller detection limits may provide enough data to test trends predicted by the models in detail.

Finally, multiannulus accretion codes are an important step towards understanding the formation and evolution of planetary systems (see also Spaute et al. 1991; Weidenschilling et al. 1997). Our calculations demonstrate that ‘complete’ disk models with 64 or more annuli evolve on faster timescales than ring models with 16 or fewer annuli. Planetesimals at the edge of a model

grid interact with fewer annuli than planetesimals in the middle of a grid. Collisional damping, dynamical friction, and runaway growth thus proceed more rapidly in a complete disk model than in a ring model. Calculations of fragmentation, gas drag, and Poynting-Robertson drag are also more accurate in a multiannulus grid. This difference is important for constructing accurate models for the formation of Jupiter and the Kuiper Belt, where observational constraints limit the mass and timescale available for planet formation (e.g., Lissauer 1987; Bailey 1994; Pollack et al. 1996; Kenyon & Luu 1999; Bryden, Lin, & Ida 2000)

We acknowledge a generous allotment,  $\sim 600$  cpu days, of computer time on the Silicon Graphics Origin-2000 ‘Alhena’ through funding from the NASA Offices of Mission to Planet Earth, Aeronautics, and Space Science. Advice and comments from M. Geller, M. Kuchner, and an anonymous referee greatly improved our presentation.

## A. APPENDIX

### A.1. Overview

We assume that planetesimals are a statistical ensemble of masses in  $N$  concentric, cylindrical annuli with width  $\Delta a_i$  and height  $H_i$  centered at radii  $a_i$  from a star with mass  $M_\star$  and luminosity  $L_\star$ . The particles have horizontal  $h_{ik}(t)$  and vertical  $v_{ik}(t)$  velocity dispersions relative to an orbit with mean Keplerian velocity  $V_{K_i}$  (Lissauer & Stewart 1993; Stewart & Ida 2000). We approximate the continuous distribution of particle masses with discrete batches having an integral number of particles  $n_{ik}(t)$  and total masses  $M_{ik}(t)$ . The average mass of each of  $M$  mass batches,  $m_{ik}(t) = M_{ik}(t)/n_{ik}(t)$ , evolves with time as collisions add and remove bodies from the batch (Wetherill & Stewart 1993).

Kenyon & Luu (1998, 1999) describe our approach for solving the evolution of particle numbers and velocities for a mass batch  $k$  in a single annulus  $i$  during a time step  $\delta t$ . Kenyon & Bromley (2001) describe our solution for the velocity evolution from elastic collisions for a set of annuli. Here we describe collision rates and velocity evolution from inelastic collisions for a set of annuli. We also include our treatment of particle loss and velocity evolution for gas drag and the Poynting-Robertson effect.

### A.2. Coagulation Equation

The coagulation equations for a particle in mass batch  $k$  of annulus  $i$  colliding with another particle in mass batch  $l$  of annulus  $j$  are

$$\delta n_{i'k'} = \delta t [\epsilon_{ijkl} A_{ijkl} n_{ik} n_{jl} - n_{i'k'} A_{i'jk'l} n_{jl}] + \delta n_{i'k',f} - \delta n_{i'k',gd} - \delta n_{i'k',prd} \quad (\text{A1})$$

$$\delta M_{i'k'} = \delta t m_{i'k'} [\epsilon_{ijkl} A_{ijkl} n_{ik} n_{jl} - n_{i'k'} A_{i'jk'l} n_{jl}] + \delta m_{i'k',f} - \delta m_{i'k',gd} - \delta m_{i'k',prd} \quad (\text{A2})$$

where  $A_{ijkl}$  is the cross-section,  $\epsilon_{ijkl} = 1/2$  for  $i = j$  and  $k = l$ , and  $\epsilon_{ijkl} = 1$  for  $k \neq l$  and any  $i, j$ . The terms in A1–A2 represent (i) mergers of  $m_{ik}$  and  $m_{jl}$  into a body of mass  $m_{i'k'} = m_{ik} + m_{jl} - m_{e,ijkl}$ , (ii) loss of  $m_{i'k'}$  through mergers with other bodies, (iii) addition of  $m_{i'k'}$  from debris produced by the collisions of other bodies, and (iv) loss of  $m_{i'k'}$  by gas drag and Poynting-Robertson drag. Kenyon & Luu (1999) outlines our calculation of the mass lost to small fragments,  $m_{e,ijkl}$ . The second term in A1–A2 includes the possibility that a collision can produce debris but no merger (rebounds; see Davis et al. 1985; Barge & Pellat 1993; Kenyon & Luu 1999, and references therein).

Following Weidenschilling et al. (1997), particles in adjacent annuli may collide if their orbits approach within 2.4 times their mutual Hill radius  $R_H$ . The ‘overlap region’ for these inelastic collisions is

$$o_{ijkl,in} = 2.4R_H + 0.5(w_{ik} + w_{jl}) - |a_i - a_j| ; \quad (\text{A3})$$

where  $w_{ik}$  is the radial extent of the orbit of particle  $k$  with orbital eccentricity  $e_k$  in annulus  $i$  (Kenyon & Bromley 2001):

$$w_{ik} = \begin{cases} \Delta a_i + e_k a_i & e_k a_i \leq \Delta a_i \\ (\Delta a_i + e_k a_i)(e_k a_i / \Delta a_i)^{1/4} & e_k a_i > \Delta a_i \end{cases} \quad (\text{A4})$$

We calculate the ‘gravitational range’ of the largest bodies –  $R_{g,ik} = K_1 a R_{H,ijkl} + 2a e_{ik}$  (Wetherill & Stewart 1993) – where  $K_1 = 2\sqrt{3}$  and  $R_{H,ijkl} = [(m_{ik} + m_{jl})/3M_\odot]^{1/3}$  is the mutual Hill radius (see also Kenyon & Luu 1998, 1999). Isolated bodies are the  $N$  largest bodies that satisfy the summation,  $\sum_{k_{min}}^{k_{max}} n_{ik} R_{g,ik} \geq \Delta a_i$  (Wetherill & Stewart 1993). These isolated bodies cannot collide with one another but can collide with other lower mass bodies in the annulus and all other bodies in other annuli.

We use the particle-in-a-box technique to calculate collision cross-sections,  $A_{ijkl}$ . Kenyon & Luu (1998) describe this approach for a calculation with a single annulus. The technique is easily generalized to a multi-annulus calculation by averaging quantities which depend on the radius of the annulus, such as the Keplerian velocity or the Hill radius (Spaute et al. 1991; Weidenschilling et al. 1997). The cross-section is

$$A_{ijkl} = \alpha_{coll} \left( \frac{1}{4 H_{ijkl} \langle a_{ij} \rangle \langle \Delta a_{ij} \rangle} \right) V_{ijkl} F_{g,ijkl} (r_{ik} + r_{jl})^2 , \quad (\text{A5})$$

where  $\alpha_{coll}$  is a constant (Wetherill & Stewart 1993; Kenyon & Luu 1998),  $H_{ijkl}$  is the mutual scale height,  $\langle a_{ij} \rangle$  and  $\langle \Delta a_{ij} \rangle$  are the average heliocentric distance and width for the two interacting annuli,  $V_{ijkl}$  is the relative particle velocity,  $F_{g,ijkl}$  is the gravitational focusing factor, and  $r_{ik}$  and  $r_{jl}$  are the particle radii. We adopt the piecewise analytic approximation of Spaute et al. (1991) for the gravitational focusing factor, and the two body collisional cross-sections of Greenberg et al. (1991) in the low velocity limit (see also Greenzweig & Lissauer 1990, 1992).

To calculate  $i'$  and  $k'$  for each collision, we establish fixed grids of annuli and masses. The radial grid has annuli with either a fixed constant size,  $\Delta a_i = a_{i+1} - a_i$ , or a variable width,  $\Delta a_i = \Delta a_0 \cdot a_i$ . The mass grid in each annulus has particle numbers  $k = 1$  to  $k = N_{max}$  with  $\delta_k = m_{k+1}/m_k$ . We set

$$\delta_k = \begin{cases} \delta_1 & k \leq k_0 \\ \delta_1 - \epsilon \cdot (k - k_0) & k_0 < k < k_1 \\ \delta_2 & k \geq k_1 \end{cases} \quad (\text{A6})$$

where  $\delta_1$ ,  $\delta_2$ , and  $\epsilon$  are constants. Grids with a fixed mass ratio between neighboring mass bins have  $\epsilon \equiv 0$ . Grids with  $\epsilon > 0$  allow coarse resolution,  $\delta \approx 1.4$ –2.0, where small objects grow slowly, and fine resolution,  $\delta \approx 1.05$ –1.4, where large objects grow rapidly. When a collision produces  $n_{k'}$  bodies with  $m_{k'}$  in annulus  $i'$ , we augment either batch  $l'$  when  $m_{k'} \leq \sqrt{m_{l'} m_{l'+1}}$  or batch  $l' + 1$  when  $m_{k'} > \sqrt{m_{l'} m_{l'+1}}$ . We add mass to annulus  $j'$  when  $f - j' < 0.5$  and to annulus  $j' + 1$  when  $f - j' \geq 0.5$ , where

$$f = \frac{im_{ik} + jm_{jl}}{m_{ik} m_{jl}}, \quad (\text{A7})$$

and  $j'$  is the integer part of  $f$ . A complete cycle through all mass batches and all annuli produces new values for  $n_{k'}$  and  $M_{k'}$  in each annulus  $i'$ , which yields new values for the average mass per bin,  $m_{k'} = M_{k'}/n_{k'}$ . This process conserves mass and provides a good description of coagulation when  $\delta_k$  is small (Ohtsuki & Nakagawa 1988; Wetherill 1990a; Ohtsuki et al. 1990; Kenyon & Luu 1998, e.g.). Our algorithm to place merged objects in a particular annulus does not conserve angular momentum specifically; test calculations conserve angular momentum to better than 1% after  $10^6$  timesteps.

### A.3. Velocity Evolution

The time evolution of particle velocities from collisional damping is

$$\frac{dh_{in,ik}^2}{dt} = \sum_{j=0}^{j=N} \sum_{l=0}^{l=l_{max}} \frac{C_{in}}{2} (m_{jl} h_{jl}^2 - m_{ik} h_{ik}^2 - (m_{ik} + m_{jl}) h_{ik}^2) I_e \quad (\text{A8})$$

$$\frac{dv_{in,ik}^2}{dt} = \sum_{j=0}^{j=N} \sum_{l=0}^{l=l_{max}} \frac{C_{in}}{\beta_{ijkl}^2} (m_{jl} v_{jl}^2 - m_{ik} v_{ik}^2 - (m_{ik} + m_{jl}) v_{ik}^2) I_i \quad (\text{A9})$$

where  $C_{in} = \alpha_{coll} f_{ijkl} \epsilon_{ijkl} \rho_{g,jl} V_{ijkl} F_{g,ijkl} (r_{ik} + r_{jl})^2$  (Hornung, Pellat, & Barge 1985; Wetherill & Stewart 1993; Ohtsuki 1992, 1999). In the second summation,  $l_{max} = k$  when  $i = j$ ;  $l_{max} = M$  when  $i \neq j$  (see also Kenyon & Luu 1998, 1999). We add a term,  $f_{ijkl}$ , to treat the overlap between adjacent zones;  $f_{ijkl} = 1$  when  $i = j$  and  $f_{ijkl} \leq 1$  when  $i \neq j$ . The integrals  $I_e$  and  $I_i$  are elliptic integrals described in previous publications (Hornung, Pellat, & Barge 1985; Wetherill & Stewart 1993; Ohtsuki 1992, 1999, Stewart & Ida 2000).

### A.4. Gas Drag

Gas drag can be an important process during the early evolution of planetesimal disks. The viscosity of the gas drags small bodies inwards through the disk and damps the motion of small bodies relative to a circular orbit. Adachi et al. (1976) and Weidenschilling (1977b) analyze the interactions between gas and planetesimals, and develop useful evolution formulae (see also

Kary, Lissauer, & Greenzweig 1993). We adopt the Adachi et al. (1976) prescription. Material drifts through an annulus at a rate

$$\frac{\delta a_{ik}}{a_i} = 2(0.97e_{ik} + 0.64i_{ik} + \eta_{ik}/V_{K,i}) \frac{\eta_i}{V_{K,i}} \frac{\delta t}{t_{d,ik}}, \quad (\text{A10})$$

where  $\eta_i$  is the gas velocity relative to the local Keplerian velocity,  $V_{K,i}$ . The characteristic drift time is

$$t_{d,ik} = \frac{365}{C_D} \left( \frac{m_{ik}}{10^{21} \text{ g}} \right)^{1/3} \left( \frac{1 \text{ AU}}{a_i} \right) \left( \frac{10^{-9} \text{ g cm}^{-3}}{\rho_{g,i}} \right) T_{K,i}, \quad (\text{A11})$$

where  $C_D = 0.5$  is the drag coefficient,  $\rho_{g,i}$  is the gas density, and  $T_{K,i}$  is the orbital period (Adachi et al. 1976; Wetherill & Stewart 1993). The removal of bodies from annulus  $i$  at each time step is then

$$\frac{\delta n_{gd,ik}}{n_{ik}} = \frac{\delta a_{ik}}{a_i}. \quad (\text{A12})$$

To specify the gas density, we adopt an initial gas-to-dust surface density ratio,  $\Sigma_{g0,i}/\Sigma_{d0,i}$ , and set  $\rho_{g0,i} = \Sigma_{g0,i}/2H_{g0,i}$ , where  $H_{g0,i}$  is the vertical scale height of the gas. We assume a scale height appropriate for a gaseous disk in hydrostatic equilibrium:

$$H_{g0,i} = H_0(a_i/a_0)^q a_i, \quad (\text{A13})$$

where  $H_0$  is the scale height at  $a_0 = 1 \text{ AU}$ . In most cases, we adopt  $H_0 = 0.05$  and  $q = 0.125$  (Kenyon & Hartmann 1987). We also assume that the gas density falls with time:

$$\rho_{g,i}(t) = \rho_{g0,i} e^{-t/t_g} \quad (\text{A14})$$

where  $t_g$  is a constant and is usually 10 Myr to 1 Gyr.

Our gas drag algorithm removes bodies from annulus  $i + 1$  and places them in annulus  $i$ . We explicitly conserve kinetic energy: the velocity dispersion of annulus  $i$  decreases as lower-velocity material is dragged inwards from outer annuli. The grid loses material and kinetic energy at the inner boundary and gains material and kinetic energy at the outer boundary. To compute the amount of material added to the grid, we assume a power-law density distribution,  $\rho_{g,i} \propto a_i^{-\alpha}$ . Equation (A12) is then  $\delta n_{gd,ik}/n_{ik} \propto a_i^{-(\alpha+0.5)}$ , where we have ignored the slow variation of  $e$ ,  $i$ , and  $\eta_i/V_{K,i}$  with  $a_i$ . The number of particles added to the last zone in the grid is:

$$\delta n'_{gd,Nk} = \left( \frac{a_N}{a_{N+1}} \right)^{\alpha+0.5} \delta n_{gd,Nk}. \quad (\text{A15})$$

The addition of kinetic energy follows

$$\delta E'_{gd,Nk} = \left( \frac{a_{Nk}}{a_{N+1k}} \right)^{\alpha+1.5} \delta E_{gd,Nk}, \quad (\text{A16})$$



where  $\delta n_{gd,Nk}$  and  $\delta E_{gd,Nk}$  are the number and kinetic energy of particles dragged inwards from annulus  $N$  to annulus  $N - 1$ .

We adopt the Wetherill & Stewart (1989) expression for velocity damping due to gas drag:

$$\frac{dV_{ik}}{dt} = \frac{-\pi C_D}{2m_{ik}} \rho_{g,i} V_{g,ik}^2 r_{ik}^2, \quad (\text{A17})$$

where  $C_D = 0.5$  is the drag coefficient and  $V_{gi} = (V_{ik}(V_{ik} + \eta_i))^{1/2}$  is the mean relative velocity of the gas.

### A.5. Poynting-Robertson Drag

When the luminosity of the central star is large, the radiation field can drag small particles towards the central star and can circularize particle velocities relative to a circular orbit. Radiation pressure can also eject very small particles from the disk. Burns, Lamy, & Soter (1979) have derived accurate expressions for these processes. Because we do not treat the evolution of the smallest grains, we ignore radiation pressure. For Poynting-Robertson drag, the inward drift of material is

$$\frac{\delta a_{ik}}{a_i} = \left( \frac{2 + 3e_{ik}^2}{(1 - e_{ik}^2)^{3/2}} \right) \frac{\eta_{pr} Q_{pr}}{a_i^2}, \quad (\text{A18})$$

where  $Q_{pr}$  is the Mie scattering coefficient and

$$\eta_{pr} = \frac{2.53 \times 10^{11}}{\rho_{ik} r_{ik}} \left( \frac{L_\star}{1 \text{ L}_\odot} \right). \quad (\text{A19})$$

The mass density of an individual grain is  $\rho_{ik}$ . The rate particles leave an annulus is

$$\frac{\delta n_{pr,ik}}{n_{ik}} = \frac{\delta a_{ik}}{a_i}. \quad (\text{A20})$$

As with gas drag, we scale the number of particles lost by annulus  $N$  to calculate the number of particles added to this zone:

$$\delta n_{pr,Nk} = \left( \frac{a_N}{a_{N+1}} \right)^2 \delta n_{pr,Nk} \quad (\text{A21})$$

For the kinetic energy:

$$\delta E'_{pr,Nk} = \left( \frac{a_{Nk}}{a_{N+1k}} \right)^3 \delta E_{pr,Nk}. \quad (\text{A22})$$

In these expressions,  $\delta n_{pr,Nk}$  and  $\delta E_{pr,Nk}$  are the number and kinetic energy of particles dragged inwards from annulus  $N$  to annulus  $N - 1$ .

We also adopt the Burns et al. (1979) expression for horizontal velocity damping from Poynting-Robertson drag,

$$\frac{\delta h_{ik}^2}{\delta t^2} = -6.25 \left( \frac{Q_{pr} h_{ik} \eta_{pr}}{a_i^2} \right)^2. \quad (\text{A23})$$

Poynting-Robertson drag does not change the vertical component of the velocity.

### A.6. Dust Luminosity and Optical Depth

To calculate the dust luminosity, we follow Kenyon et al. (1999) and estimate the bolometric luminosity reprocessed by solid objects in the disk as  $L/L_\star = \tau\Omega/4\pi$ , where  $\tau$  is the radial optical depth and  $\Omega$  is the solid angle of the disk or ring as seen from the central star. The bolometric luminosity is the sum of the thermal luminosity and the scattered light luminosity of the dust grains. For dust grains with albedo  $\omega$ , the scattered light luminosity is  $\omega L$ ; the thermal luminosity is  $(1 - \omega)L$ . These approximations assume a grey opacity and are reasonable for  $\tau \lesssim 1$ . For a disk or ring geometry, the solid angle is  $\Omega/4\pi = H/a$ , where  $H$  is the scale height and  $a$  is the radial distance from the central star.

We calculate the radial optical depth through the grid to estimate the amount of absorption and scattering of starlight by dust particles in the grid. We divide the optical depth  $\tau$  through the grid into two pieces,  $\tau_d$  measures the radial optical depth of bodies explicitly in the grid and  $\tau_s$  measures the radial optical depth of smaller bodies. We adopt the geometric optics limit for bodies with  $r_k \gg \lambda$  where  $\lambda$  is the wavelength of observation. For the large bodies in the grid:

$$\tau_d = \sum_{i=1}^N \sum_{k=2}^M N_{ik} \sigma_{ik} \Delta a_i \quad (\text{A24})$$

where  $N_{ik}$  is the number density of mass batch  $k$  in annulus  $i$  and  $\sigma_{ik}$  is the extinction cross-section. We adopt  $\sigma_{ik} = 2\pi r_{ik}^2$  and a volume  $V_{ik} = 4\pi a_i \Delta a_i H_{ik}$ . The optical depth is then independent of the width of the annulus:

$$\tau_d = \sum_{i=1}^N \sum_{k=2}^M \frac{n_{ik} r_{ik}^2}{2 a_i H_{ik}}. \quad (\text{A25})$$

For the smaller bodies, we must make assumptions about the variation of  $n$  and  $H$  with particle size. In most calculations, the vertical scale height of the dust  $H_{ik}$  is either constant or grows slowly for smaller particles. Adopting a constant  $H_{ik}$  thus maximizes the optical depth of the smallest grains. The cumulative number density usually follows  $N_C \propto r^{-\beta}$  with  $\beta \approx 2.5$  for calculations with fragmentation (Dohnanyi 1969; Williams & Wetherill 1994; Tanaka et al. 1996). Gas and Poynting-Robertson drag preferentially remove the smallest particles from the grid; these processes should lower the exponent in the number density to  $\beta \approx 1.5$  when either  $\rho_g$  or  $L_\star$  is large. Several test calculations confirm this dependence. We thus consider two cases,  $\beta = 2.5$  – when

small particles dominate the opacity and  $\beta = 1.5$  – when large particles dominate the opacity. The optical depth is then

$$\tau_s = \sum_{i=1}^N \sum_{k=1}^{-\infty} \frac{n_{i1} r_{i1}^2}{2 a_i H_{i1}} r_{ik}^{1/2} = K_\tau \sum_{i=1}^N \frac{n_{i1} r_{i1}^2}{2 a_i H_{i1}} \quad (\text{A26})$$

where

$$K_\tau = \begin{cases} 3 & \beta = 1.5 \\ 500 (r_{\min}/1 \mu\text{m})^{-1/2} & \beta = 2.5 \end{cases} \quad (\text{A27})$$

Radiation pressure limits the size of the smallest particle to radii  $\sim 1\text{--}10 \mu\text{m}$ . We plan to address the large range in possible optical depths in future studies where we explicitly calculate the evolution of small particles.

With these definitions for the optical depth, the bolometric luminosity from planetesimals in the grid is

$$L_d = \sum_{i=1}^N \sum_{k=2}^M \frac{n_{ik} r_{ik}^2}{2 a_i^2}. \quad (\text{A28})$$

This expression is independent of the scale height  $H$ . The bolometric luminosity from small particles in the grid is

$$L_{\min} = 3 \sum_{i=1}^N \frac{n_{i1} r_{i1}^2}{2 a_i^2} \quad (\text{A29})$$

in the low optical depth limit and

$$L_{\max} = 500 (r_{\min}/1 \mu\text{m})^{-1/2} \sum_{i=1}^N \frac{n_{i1} r_{i1}^2}{2 a_i^2} \quad (\text{A30})$$

in the high optical depth limit.

Krivov et al. (2000) model the dynamical evolution of two small grain populations in debris disks. They derive size distributions for grains with  $r_{ik} \lesssim 1 \text{ mm}$  for various assumptions for the collisional evolution of larger grains. Their calculations do not include velocity evolution. Krivov et al. (2000) show that collisions dominate Poynting-Robertson drag in debris disks with substantial optical depth,  $\tau \gtrsim 10^{-4}$ . If supported by calculations with velocity evolution, these results suggest that our maximum optical depth is appropriate for the early evolution of debris disk systems.

## A.7. Tests of the Evolution Code

Kenyon & Bromley (2001) describe various successful attempts to match results derived from the multi-annulus code with published calculations of velocity evolution. We have fully tested the new code in a variety of situations to verify that our algorithms conserve mass, angular momentum, and kinetic energy throughout an evolutionary sequence. The code reproduces previous results on particle growth in the Kuiper Belt (Kenyon & Luu 1999). Comparisons with previously published

calculations of terrestrial planet formation (e.g., Weidenschilling et al. 1997) will be described in a forthcoming publication.

## REFERENCES

- Adachi, I., Hayashi, C., & Nakazawa, K. 1976, *Progress of Theoretical Physics* 56, 1756
- Artymowicz, P., Burrows, C., & Paresce, F. 1989, *ApJ*, 337, 494
- Artymowicz, P. 1997, *ARE&PS*, 25, 175
- Augereau, J. C., Lagrange, A.-M., Mouillet, D., & Ménard, F. 1999, *A&A*, 350, L51
- Augereau, J. C., Lagrange, A.-M., Mouillet, D., Papaloizou, J. C. B., & Grorod, P. A. 1999, *A&A*, 348, 557
- Augereau, J. C., Nelson, R. P., Lagrange, A.-M., Papaloizou, J. C. B., & Mouillet, D. 2001, *A&A*, 370, 447
- Aumann, H. H. et al., 1984, *ApJ*, 278, L23
- Backman, D. E., & Paresce, F. 1993, in *Protostars and Planets III*, eds. E. H. Levy & J. I. Lunine, Tucson, Univ of Arizona, p. 1253
- Bailey, M. 1994, In *Asteroids, Comets, Meteors 1993*, edited by A. Milani, M. DiMartino, and A. Cellino, Kluwer Academic Publishers, Dordrecht, p. 443
- Barge, P., & Pellat, R. 1990, *Icarus*, 85, 481
- Barge, P., & Pellat, R. 1991, *Icarus*, 93, 270
- Barge, P., & Pellat, R. 1993, *Icarus*, 104, 79
- Barrado y Navascués, D., Stauffer, J. R., Song, I., & Caillault, J.-P. 1999, *ApJ*, 520, L123
- Bryden, G., Lin, D. N. C., & Ida, S. 2000, *ApJ*, 544, 481
- Burns, J. A., Lamy, P. L., & Soter, S. 1979, *Icarus*, 40, 1
- Davis, D. R., Chapman, C. R., Weidenschilling, S. J., & Greenberg, R. 1985, *Icarus*, 62, 30
- Dent, W. R. F., et al. 1995, *MNRAS*, 277, L25
- Dohnanyi, J. W. 1969, *J. Geophys. Res.*, 74, 2531
- Fajardo-Acosta, S. B., Stencel, R. E., Backman, D. E., & Thakur, N. 1999, *ApJ*, 520, 215
- Frogel, J. A., & Gould, A. 1998, *ApJ*, 499, L219
- García-Sánchez, J., Preston, R. A., Jones, D. A., Weissman, P. R., Lestrade, J.-F., Latham, D. W., & Stefanik, R. P. 1999, *AJ*, 117, 1042
- Golimowski, D. A., Durrance, S. T., & Clampin, M. 1993, *ApJ*, 411, L41

- Greaves J. S., Coulson, I. M., & Holland, W. S. 2000a, MNRAS, 312, L1
- Greaves, J. S. et al. 1998, ApJ, 506, L133
- Greaves J. S., Mannings V. & Holland, W. S. 2000b, Icarus, 143, 155
- Greenberg, R., Wacker, J. F., Hartmann, W. K., & Chapman, C. R. 1978, Icarus, 35, 1
- Greenberg, R., Weidenschilling, S. J., Chapman, C. R., & Davis, D. R. 1984, Icarus, 59, 87
- Greenberg, R., Bottke, W., Carusi, A., Valsecchi, G. B. 1991, Icarus, 94, 98
- Greenzweig, Y., & Lissauer, J. J. 1990, Icarus, 87, 40
- Greenzweig, Y., & Lissauer, J. J. 1992, Icarus, 100, 440
- Habing, H. J., et al. 1999, Nature, 401, 456
- Habing, H. J., et al. 2001, A&A, 365, 545
- Hayashi, C. 1981, Prog Theor Phys Suppl, 70, 35
- Holland, W. S., et al. 1998, Nature, 392, 788
- Hornung, P., Pellat, R., & Barge, P. 1985, Icarus, 64, 295
- Ida, S. 1990, Icarus, 88, 129
- Ida, S., Larwood, J., & Burkert, A. 2000, ApJ, 528, 351
- Ida, S., & Makino, J. 1992, Icarus, 96, 107
- Inaba, S. H., Tanaka, H., Nakazawa, K., Wetherill, G. W., & Kokubo, E. 2001, Icarus, 149, 235
- Jayawardhana, R. et al. 1998, ApJ, 503, L79
- Kalas, P., Deltorn, J.-M., & Larwood, J. 2001, ApJ, 553, 410
- Kalas, P. 1998, Earth, Moon, & Planets, 81, 27
- Kalas, P., & Jewitt, D. 1995, AJ, 110, 794
- Kalas, P., & Jewitt, D. 1997, Nature, 386, 52
- Kalas, P., Larwood, J., Smith, B. A., & Schultz, A. 2000, ApJ, 530, L133
- Kary, D. M., Lissauer, J. J., & Greenzweig, Y. 1993, Icarus, 106, 288
- Kenyon, S. J. 2002, PASP, in press
- Kenyon, S. J., & Bromley, B. C. 2001, AJ, 121, 538

- Kenyon, S. J., & Hartmann, L. 1987, *ApJ*, 323, 714
- Kenyon, S. J., & Luu, J. X. 1998, *AJ*, 115, 2136
- Kenyon, S. J., & Luu, J. X. 1999, *AJ*, 118, 1101
- Kenyon, S. J., Wood, K., Whitney, B. A., & Wolff, M. 1999, *ApJ*, 524, L119
- Kobayashi, H., & Ida, S. 2001, *astro-ph/0107086*
- Koerner, D. W., Ressler, M. E., Werner, M. W., & Backman, D. E. 1998, *ApJ*, 503, L83
- Kokubo, E., & Ida, S. 1996, *Icarus*, 123, 180
- Krivov, A. V., Mann, I., & Krivova, N. A. 2000, *A&A*, 362, 1127
- Lada, C. J. 1999, in *The Physics of Star Formation and Early Stellar Evolution*, edited by C. J. Lada and N. Kylafis, Dordrecht, Kluwer, p. 143
- Lagrange, A.-M., Backman, D., & Artymowicz, P. 2000, in *Protostars & Planets IV*, eds. V. Mannings, A. P. Boss, & S. S. Russell, Tucson, Univ. of Arizona, in press
- Larwood, J. D. 1997, *MNRAS*, 290, 490
- Larwood, J. D., & Kalas, P. G. 2001, *MNRAS*, 323, 402
- Lecavelier des Etangs, A., Vidal-Madjar, A., & Ferlet, R. 1998, *A&A*, 328, 602
- Lissauer, J. J. 1987, *Icarus*, 69, 249
- Lissauer, J. J., & Stewart, G. R. 1993, In *Protostars and Planets III*, edited by E. H. Levy and J. I. Lunine, U. of Arizona Press, Tucson, 1061
- Mouillet, D., Larwood, J. D., Papaloizou, J. C. B., & Lagrange, A.-M. 1997, *MNRAS*, 292, 896
- Nakagawa, Y., Hayashi, C., & Nakazawa, K. 1983, *Icarus*, 54, 361
- Ohtsuki, K., & Nakagawa, Y. 1988, *Prog Theor Phys (Suppl)*, 96, 239
- Ohtsuki, K., Nakagawa, Y., & Nakazawa, K. 1990, *Icarus*, 83, 205
- Ohtsuki, K. 1992, *Icarus*, 98, 20
- Ohtsuki, K. 1999, *Icarus*, 137, 152
- Pollack, J. B., Hubickyj, O., Bodenheimer, P., Lissauer, J. J., Podolak, M., & Greenzweig, Y. 1996, *Icarus*, 124, 62
- Safronov, V. S. 1969, *Evolution of the Protoplanetary Cloud and Formation of the Earth and Planets*, Nauka, Moscow [Translation 1972, NASA TT F-677]

- Schneider, G., et al. 1999, *ApJ*, 513, L127
- Smith, B. A., & Terrile, R. J. 1984, *Science*, 226, 1421
- Song, I., Caillault, J.-P., Barrado y Navascués, D., & Stauffer, J. R. 2000a, *ApJ*, 546, 352
- Song, I., Caillault, J.-P., Barrado y Navascués, D., Stauffer, J. R., & Randich, S. 2000b, *ApJ*, 533, L41
- Spangler, C., Sargent, A. I., Silverstone, M. D., Becklin, E. E., & Zuckerman, B. 2001, *ApJ*, 555, 932
- Spaute, D., Weidenschilling, S. J., Davis, D. R., & Marzari, F. 1991, *Icarus*, 92, 147
- Stern, S. A., & Colwell, J. E. 1997a, *AJ*, 114, 841
- Stern, S. A., & Colwell, J. E. 1997b, *ApJ*, 490, 879
- Stewart, G. R., & Ida, S. 2000, *Icarus*, 143, 28
- Tanaka, H., Inaba, S., & Nakazawa, K. 1996, *Icarus*, 123, 450
- Thi, W. F., et al. 2001, *Nature*, 409, 60
- Weidenschilling, S. J. 1977a, *Astrophys Sp Sci*, 51, 153
- Weidenschilling, S. J. 1977b, *MNRAS*, 180, 57
- Weidenschilling, S. J., Spaute, D., Davis, D. R., Marzari, F., & Ohtsuki, K. 1997, *Icarus*, 128, 429
- Weinberger, A. J., Becklin, E. E., Schneider, G., Smith, B. A., Lowrance, P. J., Silverstone, M. D., Zuckerman, B., Terrile, R. J. 1999, *ApJ*, 525, L53
- Wetherill, G. W. 1980, *ARA&A*, 18, 77
- Wetherill, G. W. 1990a, *Icarus*, 88, 336
- Wetherill, G. W. 1990b, *ARE&PS*, 18, 205
- Wetherill, G. W., & Stewart, G. R. 1989, *Icarus* 77, 300
- Wetherill, G. W., & Stewart, G. R. 1993, *Icarus*, 106, 190
- Williams, D. R., & Wetherill, G. W. 1994, *Icarus*, 107, 117
- Zuckerman, B., Forveille, T., & Kastner, J. H. 1995, *Nature*, 373, 494



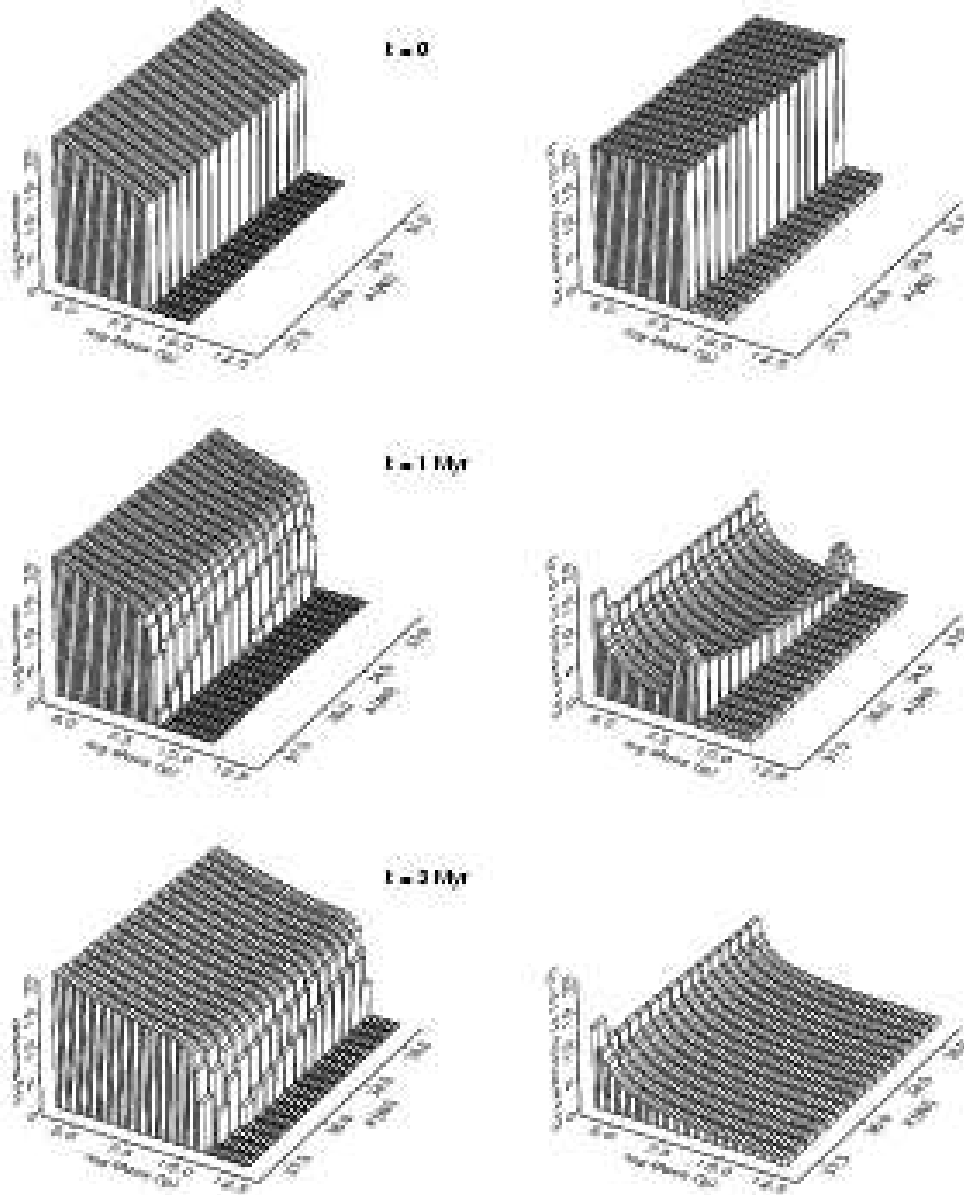


Fig. 1.— Evolution of particle number (left panels) and eccentricity (right panels) for planetesimals in orbit around a  $3 M_{\odot}$  star at 35 AU. The sixteen annuli in the grid for this ring model contain planetesimals with  $r_0 = 0.1\text{--}10$  m,  $e_0 = 2 \times 10^{-2}$ ,  $N(m) \propto m^{-1}$ , and a total mass of  $0.667 M_{\oplus}$  at  $t = 0$  (top two panels). The middle panels show the particle number and eccentricity at  $t = 1$  Myr; the bottom panels show the particle number and eccentricity at  $t = 3$  Myr. Despite considerable mass loss from shattering, collisional damping reduces the orbital eccentricities to  $\sim 10^{-3}$  on timescales of 1–10 Myr. Low velocity collisions then promote growth of larger objects through mergers. Style adapted from Weidenschilling et al. (1997).

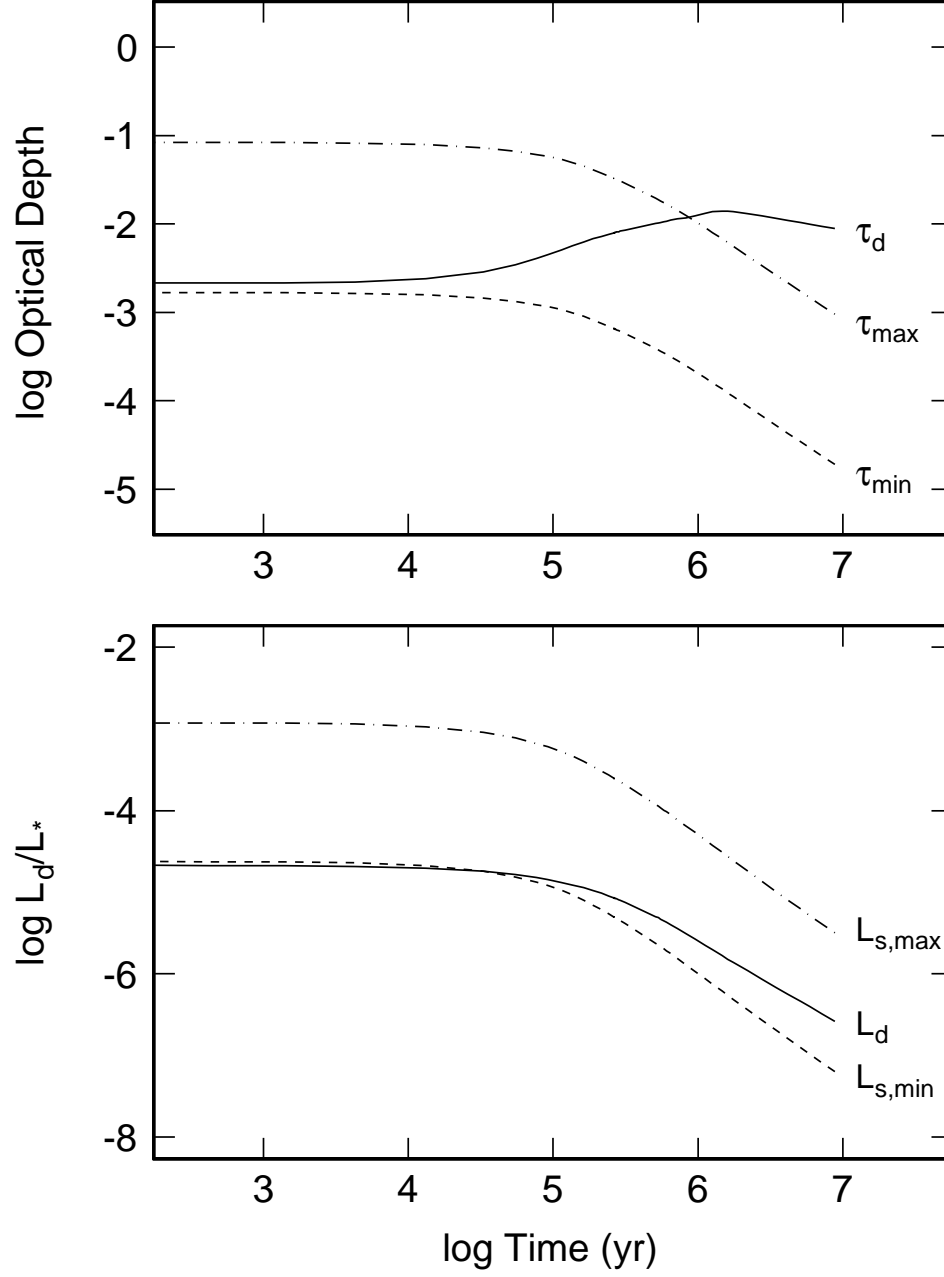


Fig. 2.— Evolution of optical depth (upper panel) and reprocessed luminosity (lower panel) for the ring model of Figure 1.

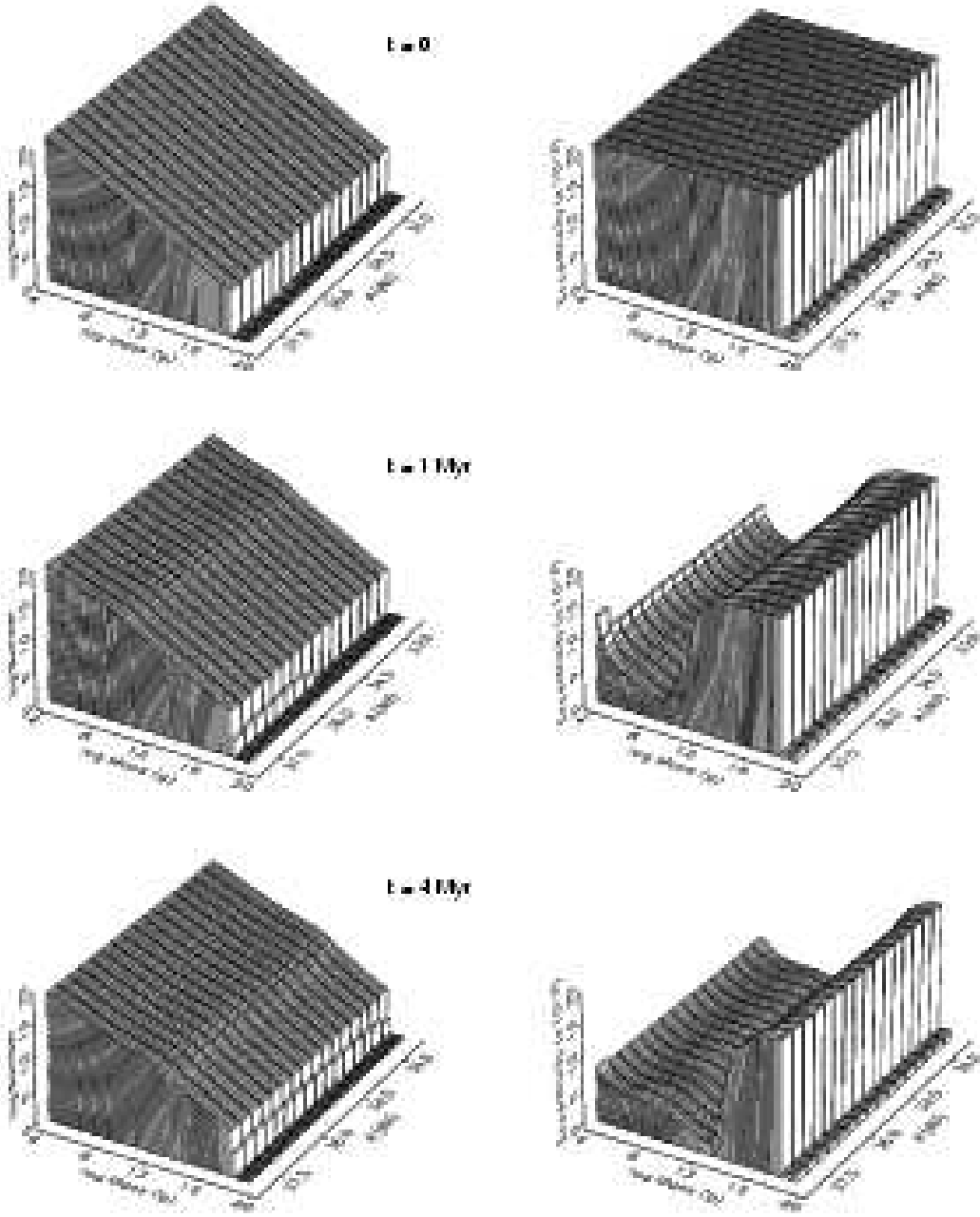


Fig. 3.— As in Figure 1, for planetesimals with  $r_{max} = 10 \text{ km}$  at  $t = 0$  (top panels),  $t = 1 \text{ Myr}$  (middle panels), and  $t = 4 \text{ Myr}$  (bottom panels).

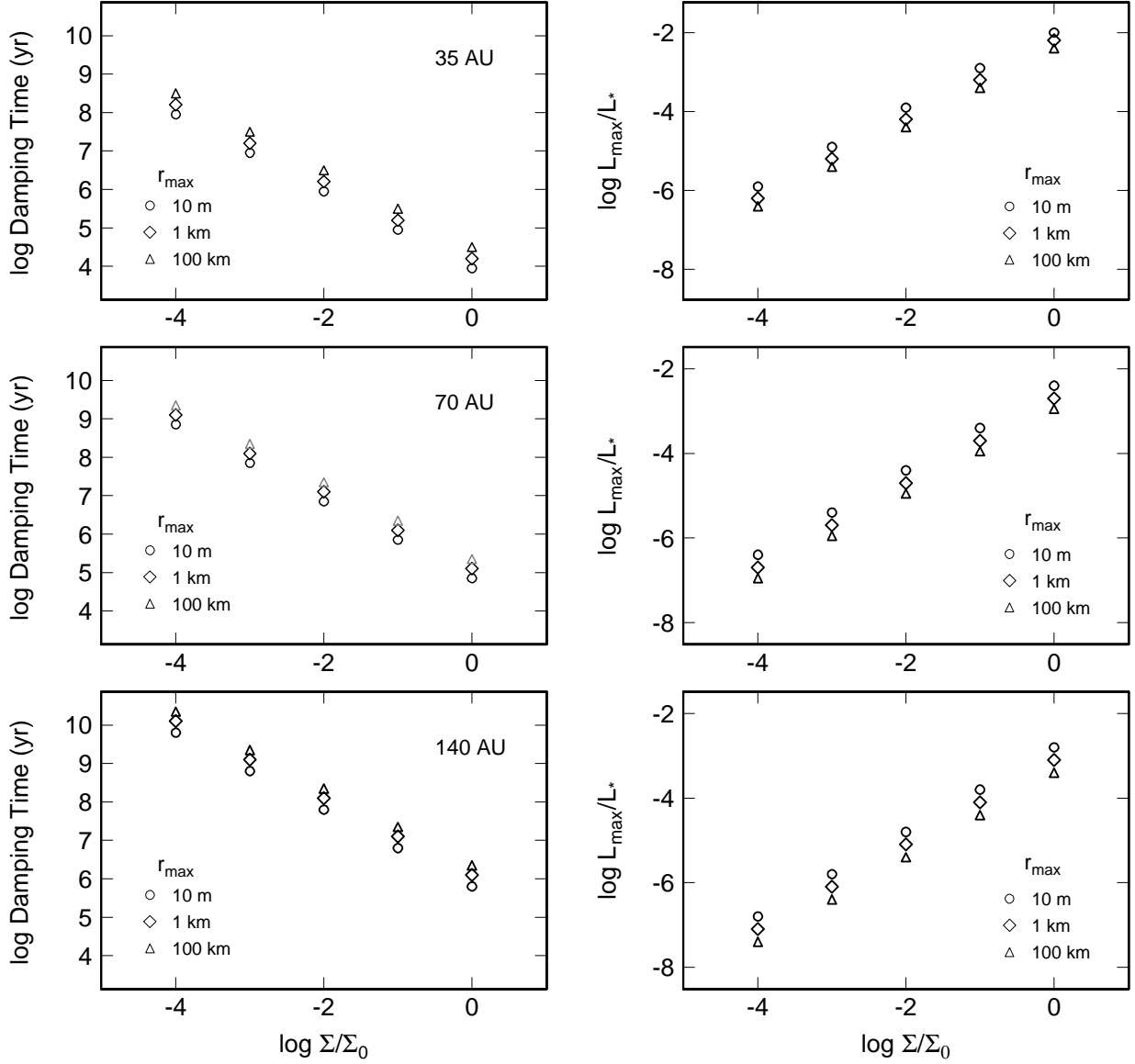


Fig. 4.— Damping time (left panels) and dust luminosity (right panels) as a function of initial surface density for ring models at 35, 70, and 140 AU. Models with  $\Sigma = \Sigma_0$  have surface densities of solid material similar to a minimum mass solar nebula. All models have  $r_{\min} = 10$  cm; model results for different values of  $r_{\max}$  are shown as indicated by the legend in each panel.

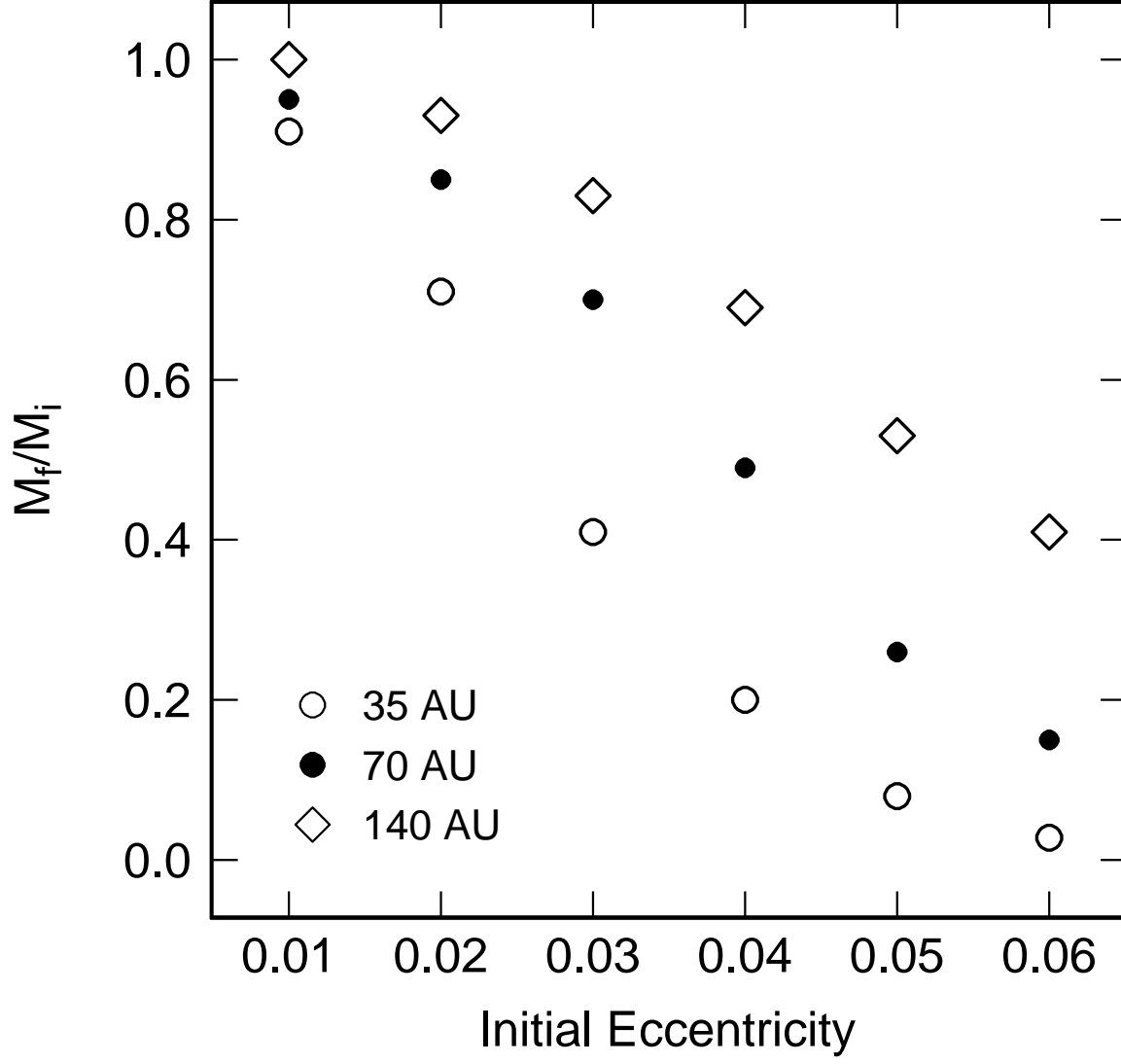


Fig. 5.— The ratio of final mass,  $M_f$ , to the initial mass,  $M_i$ , as a function of the initial eccentricity for ring models at 35 AU (open circles), 70 AU (filled circles), and 140 AU (open diamonds). Models with large  $e_0$  lose most of their mass.

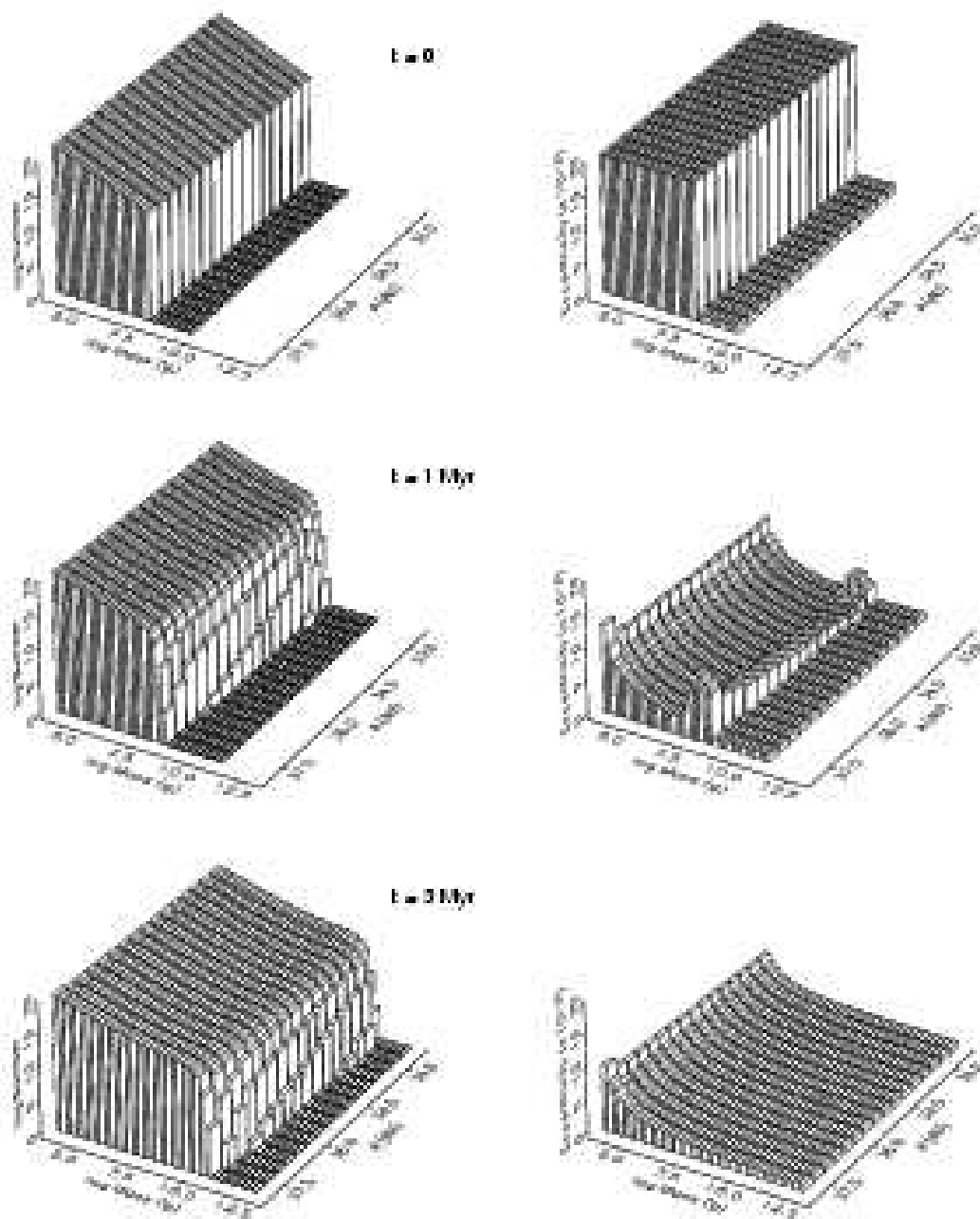


Fig. 6.— As in Figure 1, for a ring model with gas drag. The initial gas to dust mass ratio is 10:1.

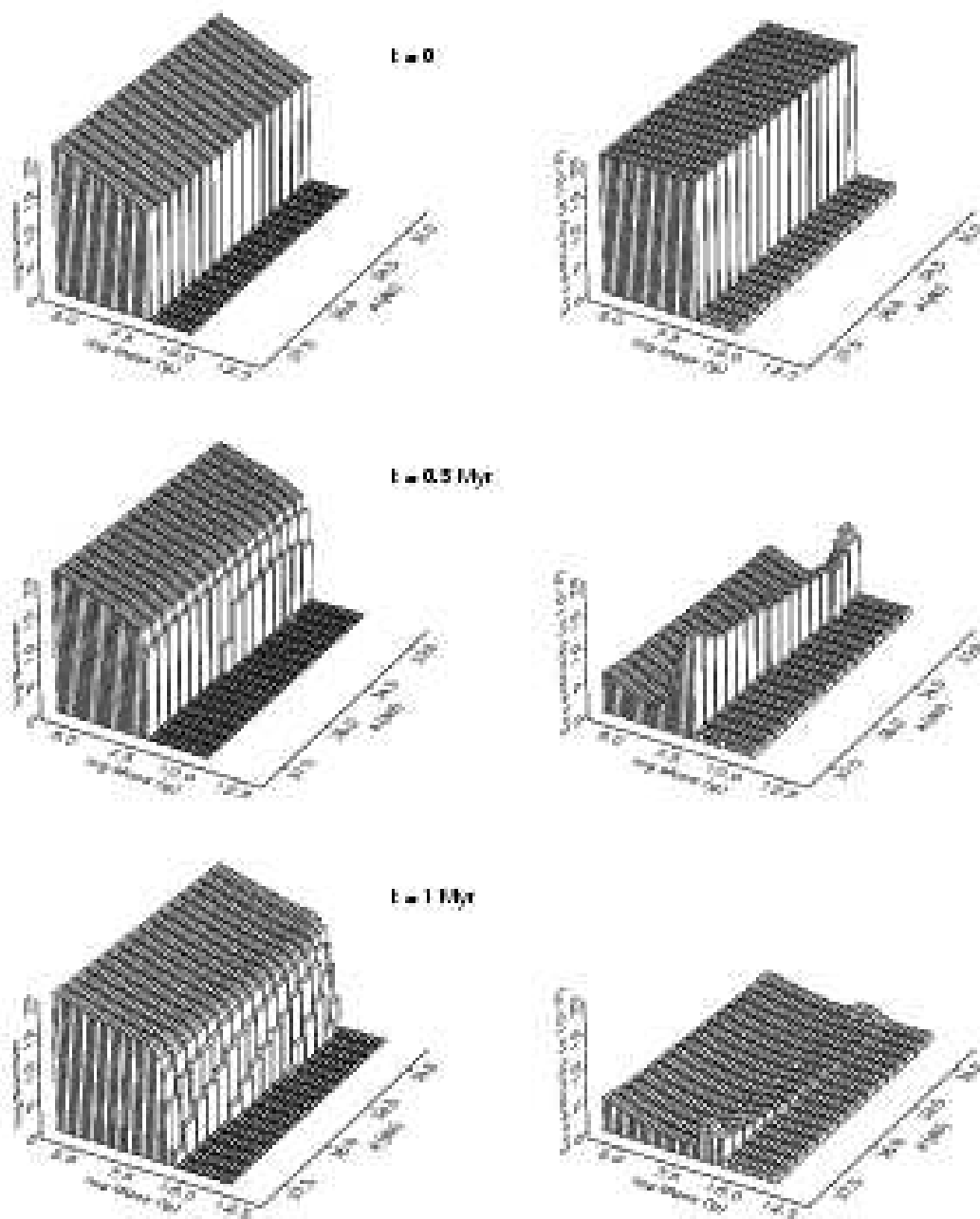


Fig. 7.— As in Figure 6, for a ring model with an initial gas to dust mass ratio of 100:1.

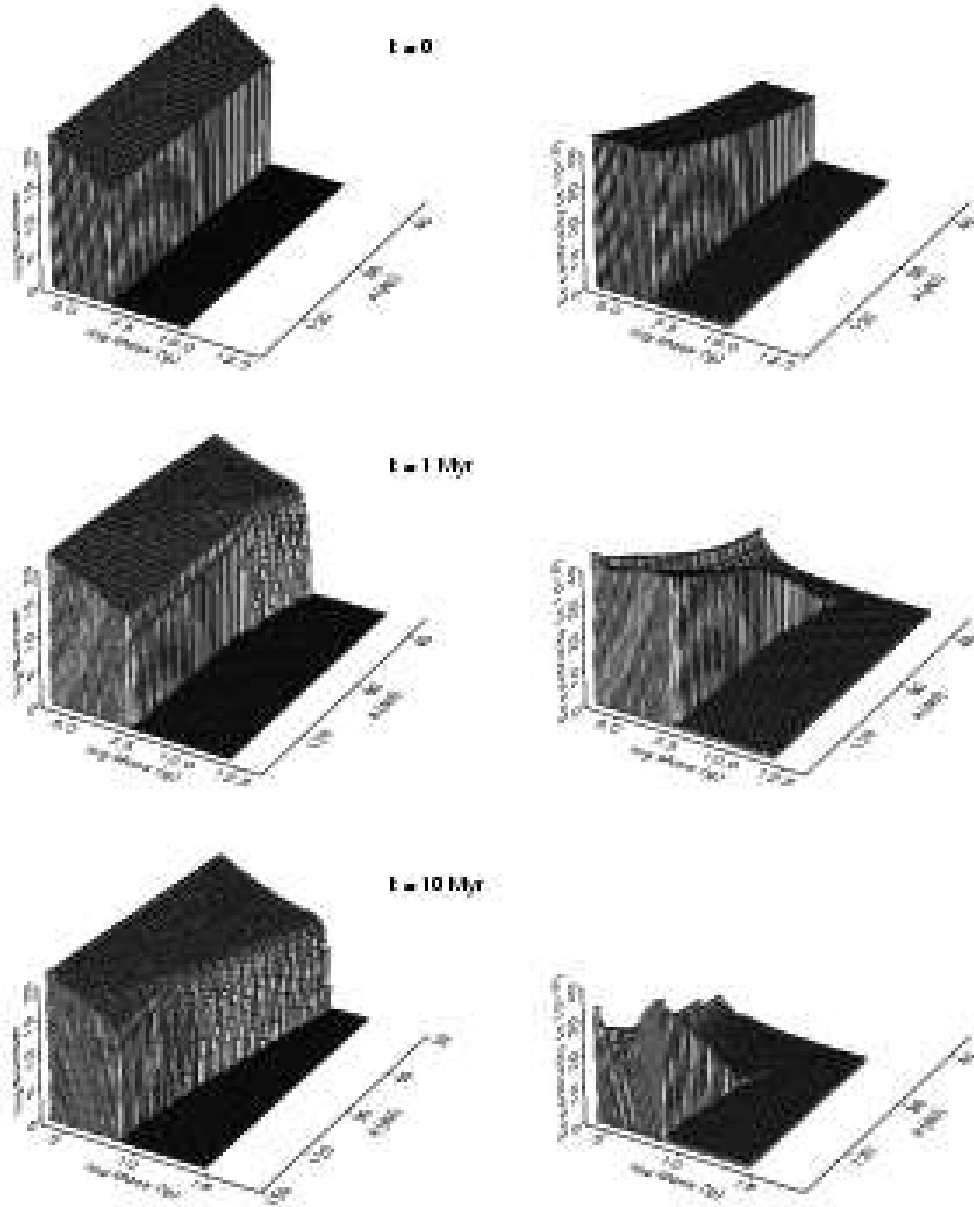


Fig. 8.— Evolution of particle number (left panels) and eccentricity (right panels) for planetesimals in orbit around a  $3 M_{\odot}$  star at 30–150 AU. The 64 annuli in the model grid contain planetesimals with  $r_0 = 0.1\text{--}10$  m,  $e_0 = 2 \times 10^{-2}$ ,  $N(m) \propto m^{-1}$ , and a total mass of  $10 M_{\oplus}$  at  $t = 0$  (top two panels). The model grid extends from 30 AU at the inner edge to  $\sim 150$  AU at the outer edge. Despite considerable mass loss from shattering, collisional damping reduces the orbital eccentricities to  $\sim 10^{-3}$  on timescales of 1–10 Myr. Low velocity collisions then promote growth of larger objects through mergers.



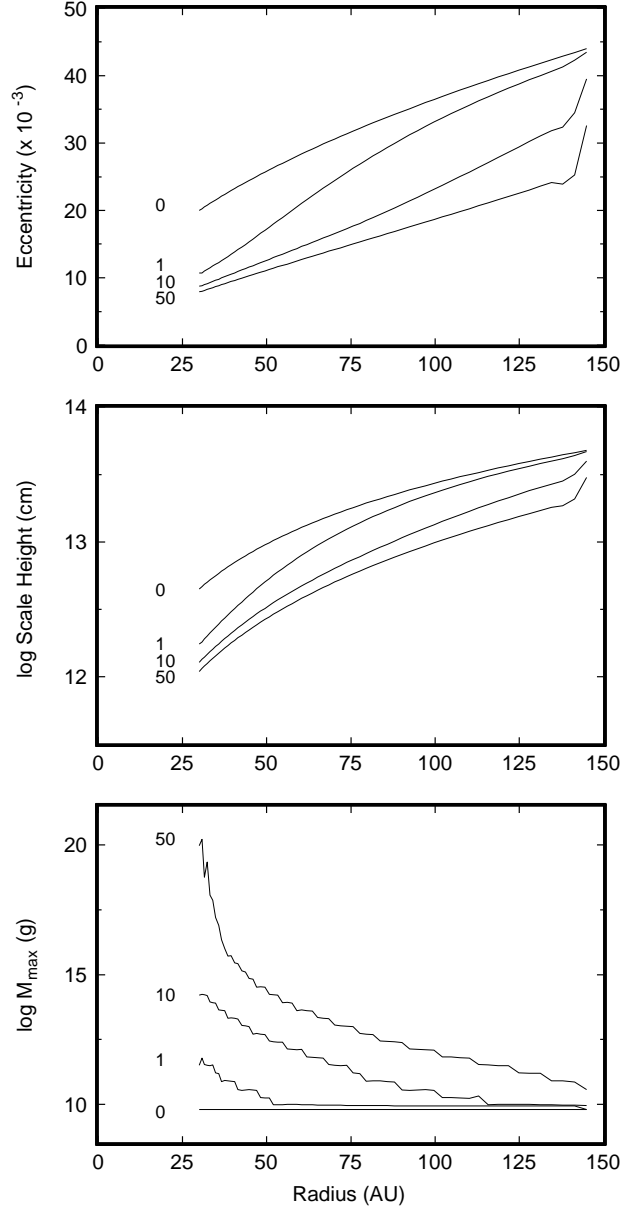


Fig. 9.— Evolution of the smallest and largest bodies in the full disk model of Figure 8. Top panel: eccentricity of the smallest bodies,  $r_k = 10$  cm, as a function of disk radius at  $t = 0, 1, 10$ , and  $50$  Myr. The abrupt rise in  $e$  at the outer edge of the grid is a numerical artifact. Middle panel: scale height of bodies with  $r_k = 10$  cm as a function of disk radius at  $t = 0, 1, 10$ , and  $50$  Myr. Bottom panel: mass of the largest body in each annulus at  $t = 0, 1, 10$ , and  $50$  Myr. Large bodies at the inner edge of the grid are starting the runaway growth phase just as growth begins at the outer edge of the grid.

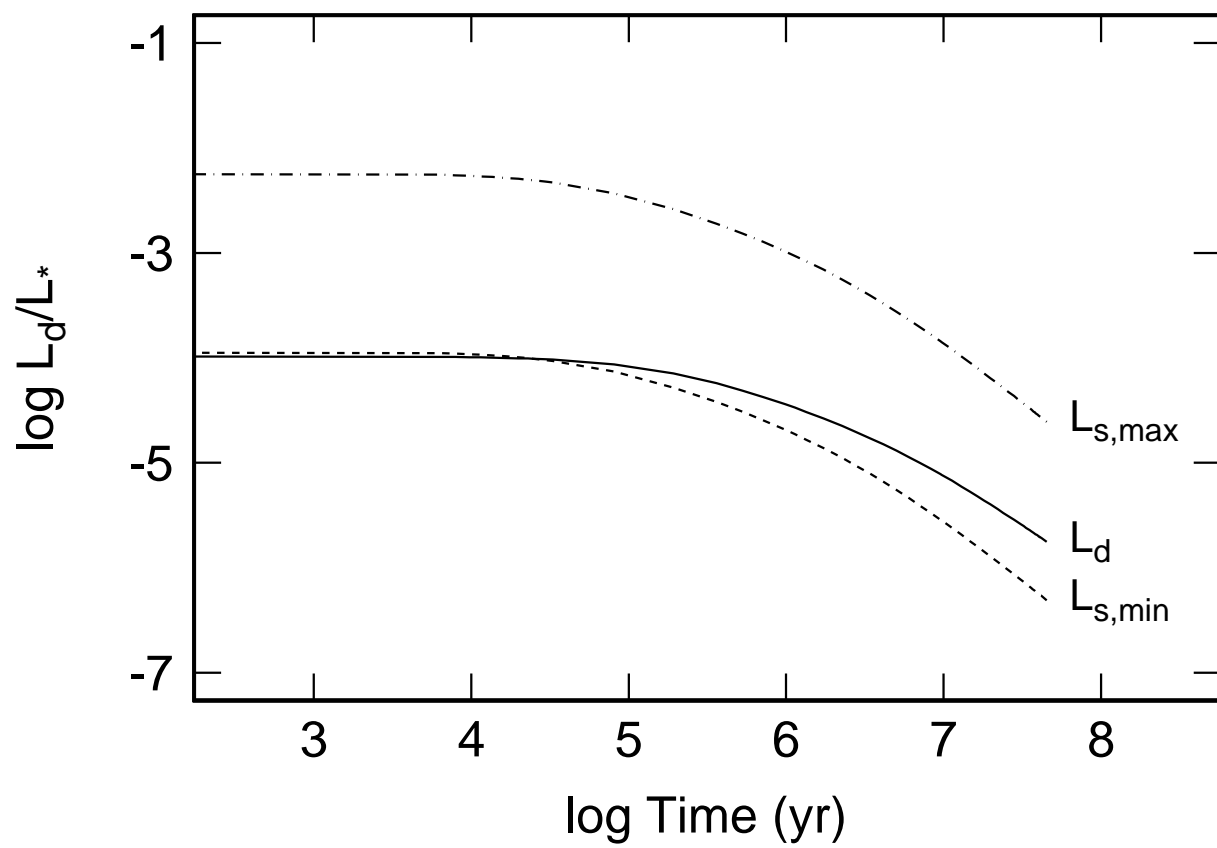


Fig. 10.— Evolution of dust luminosity for the full disk model of Figure 8.

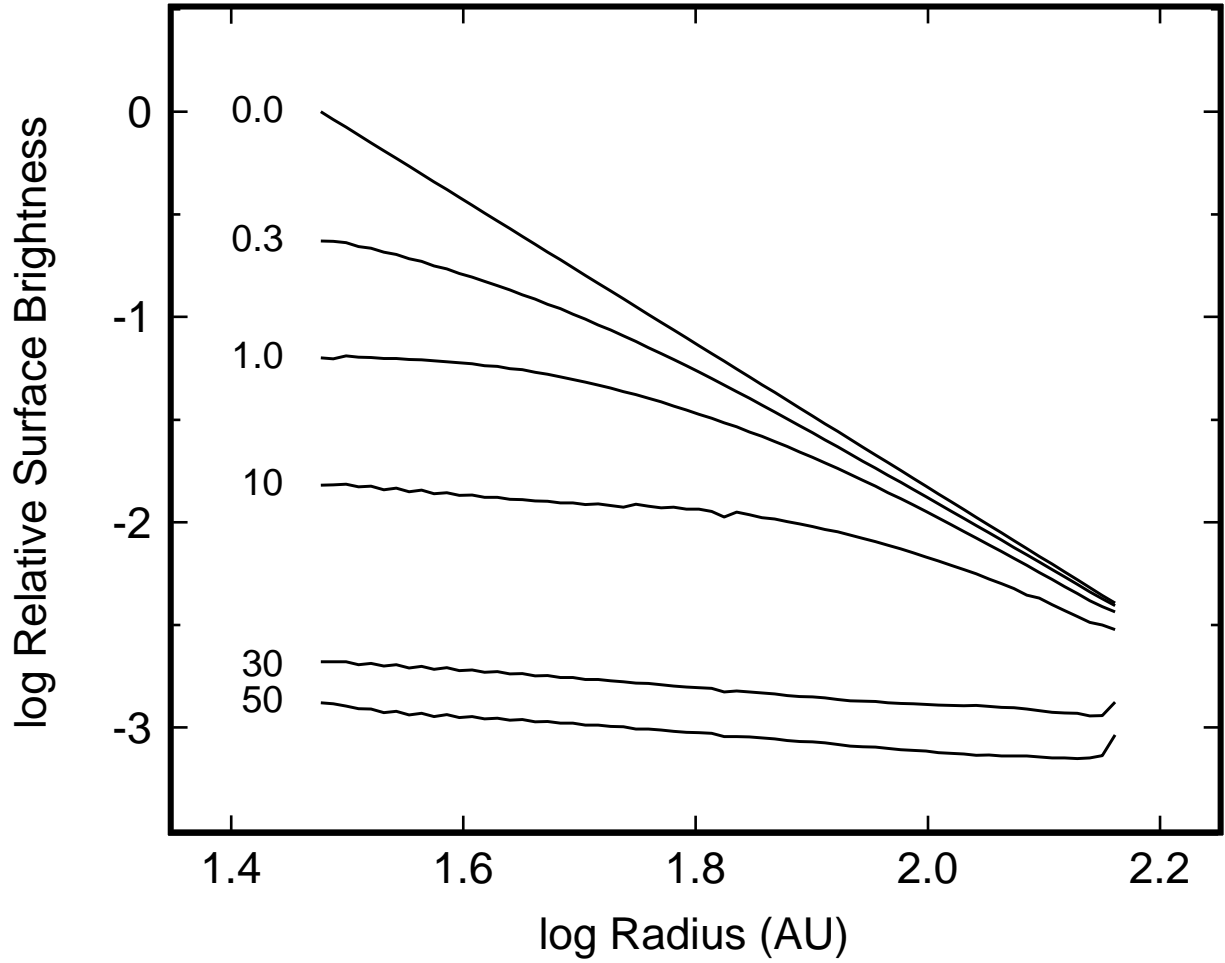


Fig. 11.— Evolution of surface brightness for the full disk model of Figure 8. At  $t = 0$ , the surface brightness profile is a power law,  $I \propto a_i^{-p}$ , with  $p = 3.5$ . For  $t = 0$ –1 Myr, the surface brightness at the inner edge of the disk fades by an order of magnitude; the surface brightness at the outer edge,  $\log r_i \gtrsim 1.8$ –2.0, barely changes. The outer edge of the disk begins to fade at  $t = 1$ –10 Myr. For  $t = 10$ –50 Myr, the entire disk fades by an order of magnitude, and begins to produce planets. For  $t = 30$  Myr and 50 Myr, the rise in surface brightness at the outer edge of the disk is a numerical artifact.

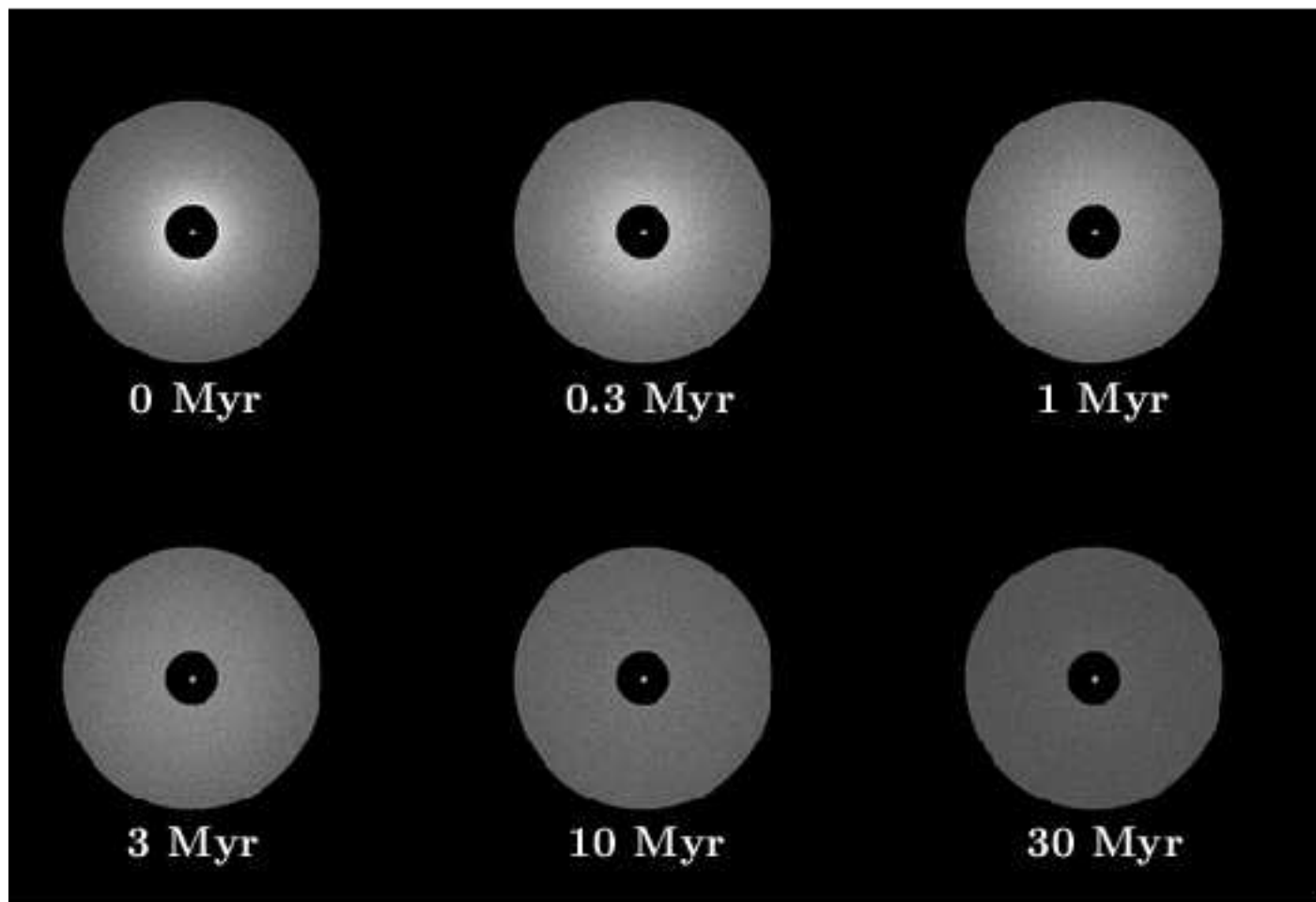


Fig. 12.— Model images for the full disk calculation of Figure 8. The panels show surface brightness distributions in the disk at selected times in the calculation.